J Biomol NMR (2012) 54:355–376
DOI 10.1007/s10858-012-9678-6

ARTICLE

Accuracy and precision of protein–ligand interaction kinetics determined from chemical shift titrations

Craig J. Markin · Leo Spyracopoulos

Received: 10 July 2012 / Accepted: 10 October 2012 / Published online: 21 October 2012

Abstract NMR-monitored chemical shift titrations for the study of weak protein–ligand interactions represent a rich source of information regarding thermodynamic parameters such as dissociation constants (K_D) in the micro- to millimolar range, populations for the free and ligand-bound states, and the kinetics of interconversion between states, which are typically within the fast exchange regime on the NMR timescale. We recently developed two chemical shift titration methods wherein co-variation of the total protein and ligand concentrations gives increased precision for the K_D value of a 1:1 protein–ligand interaction (Markin and Spyracopoulos in J Biomol NMR 53: 125–138, 2012). In this study, we demonstrate that classical line shape analysis applied to a single set of ^{1}H–^{15}N 2D HSQC NMR spectra acquired using precise protein–ligand chemical shift titration methods we developed, produces accurate and precise kinetic parameters such as the off-rate (k_{off}). For experimentally determined kinetics in the fast exchange regime on the NMR timescale, $k_{off} \sim 3{,}000\ s^{-1}$ in this work, the accuracy of classical line shape analysis was determined to be better than 5 % by conducting quantum mechanical NMR simulations of the chemical shift titration methods with the magnetic resonance toolkit GAMMA. Using Monte Carlo simulations, the experimental precision for k_{off} from line shape analysis of NMR spectra was determined to be 13 %, in agreement with the theoretical precision of 12 % from line shape analysis of the GAMMA simulations in the presence of noise and protein concentration errors. In addition, GAMMA simulations were employed to demonstrate that line shape analysis has the potential to provide reasonably accurate and precise k_{off} values over a wide range, from 100 to 15,000 s^{-1}. The validity of line shape analysis for k_{off} values approaching intermediate exchange ($\sim 100\ s^{-1}$), may be facilitated by more accurate K_D measurements from NMR-monitored chemical shift titrations, for which the dependence of K_D on the chemical shift difference ($\Delta\omega$) between free and bound states is extrapolated to $\Delta\omega = 0$. The demonstrated accuracy and precision for k_{off} will be valuable for the interpretation of biological kinetics in weakly interacting protein–protein networks, where a small change in the magnitude of the underlying kinetics of a given pathway may lead to large changes in the associated downstream signaling cascade.

Keywords Chemical shift titration · Chemical exchange rate · Protein–protein interaction · Protein–ligand interaction

C. J. Markin · L. Spyracopoulos (✉)
Department of Biochemistry, University of Alberta, Edmonton, AB T6G 2H7, Canada
e-mail: leo.spyracopoulos@ualberta.ca

Introduction

Weak protein–protein interactions with fast kinetics are fundamental for the temporal flow of information in signaling networks, regulating varied life processes such as DNA repair (Petrini 2007), innate immunity (Covert et al. 2005), and trafficking (Haglund et al. 2003). From its inception, NMR spectroscopy has played a vital role as an enabling technology for the analysis of molecular architecture and dynamics; allowing for pioneering investigations of the thermodynamics and kinetics of chemical exchange in small molecule systems (Gutowsky and Saika 1953; Rogers and Woodbrey 1962), as well as the binding of the protein serum albumin to penicillin G (Fischer and Jardetzky 1965), through chemical shift titration and line shape analysis.

Traditionally, line shape analysis has involved application of the Bloch equations, derived using classical physics, to describe the motion of nuclear spins, with general modifications to include the effects of chemical exchange (McConnell 1958). Such a phenomenological approach is limited however, in that classical line shape equations are not applicable to coupled spin systems, and may lead to inaccurate kinetics, particularly for high-resolution NMR spectra of small molecules (Binsch 1969; Rao 1989). To address this limitation, a unified quantum mechanical theory for the description of NMR line shapes in the presence of chemical exchange has been developed (Binsch 1969). However, in the absence of spin–spin couplings, the modified Bloch equations are equivalent to quantum mechanical formulations (Bain 2003).

For macromolecular systems, early line shape applications involved one dimensional ^{1}H or heteronuclear NMR spectroscopy with analyses using the Bloch equations or the density matrix approach (Baldo et al. 1975; Vasavada et al. 1980; Shriver and Sykes 1981; Kern et al. 1995; Schmitt et al. 1995; Johnson et al. 1998). The advent of multidimensional, heteronuclear NMR spectroscopy has allowed for the study of the structures and dynamics of proteins of moderate size ($\sim$30 kDa) (Bax and Grzesiek 1993). Subsequent methodological advances have extended the applicability of NMR to proteins in the 100 kDa range (Tugarinov and Kay 2005; Gelis et al. 2007). Blending multidimensional, heteronuclear NMR methods with chemical shift titrations and line shape analysis has provided detailed insights into the thermodynamics and kinetics of diverse biological processes and molecular recognition events (McKay et al. 1999; Korchuganov et al. 2001; Günther and Schaffhausen 2002; Tugarinov and Kay 2003; Rintala-Dempsey et al. 2006; Marintchev et al. 2007; Markin et al. 2010a; Greenwood et al. 2011; Lian and Roberts 2011; Arai et al. 2012).

The potential of utilizing multidimensional heteronuclear NMR methods such as the ubiquitous ^{1}H–^{15}N HSQC NMR experiment (Morris and Freeman 1979; Bodenhausen and Ruben 1980; Palmer et al. 1991; Kay et al. 1992) to determine both thermodynamic quantities such as dissociation constants (populations), and kinetics from a single set of spectra corresponding to a protein–protein or protein–ligand titration is alluring. It is noteworthy that line shape analysis is particularly valuable for the study of molecular recognition events in the fast exchange regime ($k_{ex} \gg |\Delta\omega|$), given that values for populations and rates can be determined. Furthermore, line shape analysis facilitates the identification and evaluation of multi-state binding equilibria (Kovrigin 2012). However, the general consensus is that line shape analysis is mainly a qualitative, or semi-quantitative method, on account of caveats that it is unlikely to be practical for large proteins, and that limited digital resolution in heteronuclear experiments leads to inaccurate kinetics (Palmer et al. 2001; Lian and Roberts 2011). In addition to these caveats, care must be taken to account for differential intensity losses between the HSQC spectra of a titration due to relaxation and exchange during INEPT polarization transfers, as well as during the collection of two-dimensional spectra (Günther and Schaffhausen 2002; Tugarinov and Kay 2003). Furthermore, the accuracy of the kinetics obtained from line shape analysis is dependent upon the accuracy of the intrinsic transverse relaxation rates (R_2^0), or line widths ($\Delta\nu_{1/2} = R_2^0/\pi$) of the exchanging resonance peaks, and the accuracy of the K_D value when it is determined separately and employed in the line shape analysis through the relationship $K_D = k_{off}/k_{on}$.

We recently developed 2D ^{1}H–^{15}N HSQC NMR-monitored chemical shift titration methods wherein co-variation of the total protein and ligand concentrations allow for the determination of precise K_D values for 1:1 protein–protein interactions with kinetics in the fast exchange regime (Markin and Spyracopoulos 2012). The methodology was applied to study the interaction of human ubiquitin (76 residues) with the human ubiquitin binding protein [U–^{15}N]-Mms2 (145 residues). In this study, we demonstrate that classical line shape analysis applied to the same set of 2D ^{1}H–^{15}N HSQC NMR spectra from our previous chemical shift titrations (Markin and Spyracopoulos 2012), yields accurate (<5 %) and precise ($\sim$13 %) experimental off-rates (k_{off}) in the range of $\sim$3,000 s^{-1} for 1:1 protein–protein ligand interactions.

The accuracy of line shape analysis was determined by conducting quantum mechanical NMR simulations of the chemical shift titration methods with the magnetic resonance toolkit GAMMA (Smith et al. 1994). For these theoretical simulations, the inclusion of concentration errors for line shape fitting, as well as the addition of noise to FIDs calculated with GAMMA, allowed us to conduct Monte Carlo simulations to evaluate the theoretical precision for k_{off} determined using classical line shape analysis, for the 1:1 interaction between ubiquitin and Mms2. The experimental precision for k_{off} was also determined using Monte Carlo simulations, wherein the main sources of experimental error were assumed to arise from concentration errors and noise in the FID. The consistency between the theoretical and experimental precision and the standard deviation for the per residue k_{off} values indicates that the main sources of random error in the line shape analyses arise from concentration error and the thermal electromotive force (noise) in the NMR probe coil. In addition, the magnitude of the accuracy and precision from Monte Carlo trials of the GAMMA simulations indicate that the typical digital resolution for the direct and indirect dimensions of 2D ^{1}H–^{15}N HSQC NMR spectra is not an impediment to

accurate and precise line shape analysis. We also demonstrate that systematic errors in R_2^0 and K_D do not seriously compromise the accuracy of the fitted k_{off} from classical line shape analysis as implemented in this study. We also designed a number of GAMMA simulations to determine that the accuracy and precision of classical line shape analysis over a range of k_{off} from 100 to 15,000 s^{-1} is reasonable. Finally, we show that the applicability of line shape analyses for k_{off} values in the intermediate exchange regime can be facilitated by more accurate K_D values obtained from chemical shift titrations. For these NMR-monitored chemical shift titrations, extrapolation of the theoretical dependence of K_D values on the chemical shift difference between the free and bound states to $\Delta\omega = 0$ leads to more accurate K_D values.

Theory and methods

Chemical exchange for 1:1 protein–ligand interactions

The interaction between a protein and cognate ligand to form a protein–ligand complex is given by the reaction (Hammes 2000; Palmer et al. 2001):

$$\mathrm{P} + \mathrm{L} \underset{k_{off}}{\overset{k_{on}[\mathrm{L}]}{\rightleftharpoons}} \mathrm{PL} \tag{1}$$

where P, L, and PL are the concentrations of free protein, free ligand, and protein–ligand complex, respectively, k_{on} is the on-rate constant for association of ligand and protein, and k_{off} is the off-rate constant for the ligand from the complex. Subsequent to initial mixing of protein and ligand, equilibrium is reached. Equation 1 describes chemical exchange between two sites, in this case, the free and bound states of a protein. In the absence of scalar coupling, the Bloch equations as modified by McConnell provide a rigorous description of the NMR line shape for a two-site system undergoing chemical exchange; the time-dependence of the transverse magnetization is given by (Palmer et al. 2001):

$$\begin{aligned} M_A(t) &= M_A(0)a_{11}(t) + M_B(0)a_{12}(t) \\ M_B(t) &= M_B(0)a_{22}(t) + M_A(0)a_{21}(t) \end{aligned} \tag{2}$$

for spins A and B, with coefficients:

$$a_{11}(t) = \frac{1}{2}\left[\begin{array}{l} \left(1 - \dfrac{-i\Delta\omega + R_{2A}^0 - R_{2B}^0 + k_{ex}(p_B - p_A)}{\lambda_+ - \lambda_-}\right)\exp(-\lambda_- t) \\ +\left(1 + \dfrac{-i\Delta\omega + R_{2A}^0 - R_{2B}^0 + k_{ex}(p_B - p_A)}{\lambda_+ - \lambda_-}\right)\exp(-\lambda_+ t) \end{array}\right] \tag{3}$$

$$a_{22}(t) = \frac{1}{2}\left[\begin{array}{l} \left(1 + \dfrac{-i\Delta\omega + R_{2A}^0 - R_{2B}^0 + k_{ex}(p_B - p_A)}{\lambda_+ - \lambda_-}\right)\exp(-\lambda_- t) \\ +\left(1 - \dfrac{-i\Delta\omega + R_{2A}^0 - R_{2B}^0 + k_{ex}(p_B - p_A)}{\lambda_+ - \lambda_-}\right)\exp(-\lambda_+ t) \end{array}\right] \tag{4}$$

$$a_{12}(t) = \frac{k_{ex}\,p_A}{\lambda_+ - \lambda_-}\left[\exp(-\lambda_- t) - \exp(-\lambda_+ t)\right] \tag{5}$$

$$a_{21}(t) = \frac{k_{ex}\,p_B}{\lambda_+ - \lambda_-}\left[\exp(-\lambda_- t) - \exp(-\lambda_+ t)\right] \tag{6}$$

In the absence of chemical exchange, R_{2A}^0 and R_{2B}^0 are the intrinsic transverse relaxation rates for spins A and B, respectively, $\Delta\omega$ is the difference between the chemical shifts of spin A (Ω_A) and spin B (Ω_B) in rad s^{-1}, the rate of chemical exchange is given by $k_{ex} = k_{on}[\mathrm{B}] + k_{off}$, p_A and p_B are the populations of spin A and B, respectively, and

$$\lambda_\pm = \frac{1}{2}\left[\begin{array}{l} -i\Omega_A - i\Omega_B + R_{2A}^0 + R_{2B}^0 + k_{ex} \\ \pm\sqrt{\left(-i\Delta\omega + R_{2A}^0 - R_{2B}^0 + k_{ex}(p_B - p_A)\right)^2 + 4p_A p_B k_{ex}^2} \end{array}\right] \tag{7}$$

The NMR line shape for a two-spins-1/2 system without scalar couplings, derived from the Bloch-McConnell equations, is equivalent to that calculated using a quantum mechanical density matrix approach (Bain 2003). In the absence of FID truncation and post-acquisition processing, NMR spectra from chemical shift titrations can be fit to the Fourier transforms of the sum of the auto- and cross-correlation peaks (Eq. 2), or similar frequency domain expressions (Sutherland 1972), to estimate the value of k_{ex}.

NMR simulations of chemical shift titrations with GAMMA

We recently developed two chemical shift titration methods by which precise protein–ligand dissociation constants (K_D) can be derived through co-variation of the total protein and ligand concentrations (Markin and Spyracopoulos 2012). The first, Method 1, involves addition of aliquots of concentrated ligand solution to a concentrated protein solution with concomitant decreases in protein concentration by a constant factor. Method 2 involves the sequential dilution of a solution of concentrated ligand and protein, in an initial ~2:1 ratio. To assess the accuracy and precision of these methods with respect to the determination of kinetic parameters such as the k_{off} rate constant in Eq. 1, we used the magnetic resonance toolkit GAMMA to perform quantum–mechanical simulations (Smith et al. 1994).

Simulations were designed to produce ^{1}H line shapes similar, but not identical, to experimentally observed line shapes for the W33 side chain $^{1}H_{\varepsilon 1}$ in human Mms2 upon titration with human Ub (Markin and Spyracopoulos 2012). A five spins-1/2 system was employed, and included the scalar coupled indole $^{15}N_{\varepsilon 1}$–$^{1}H_{\varepsilon 1}$ pair (^{1}J was set to 93 Hz, though the actual value is slightly larger at 99 Hz), and three protons within 3 Å of the indole proton from the crystallographically determined structure of Mms2. One-dimensional ^{1}H NMR spectra at a Larmor frequency of 600 MHz (magnetic field strength of 14.1 Tesla) were simulated with the OverBodenhausen pulse sequence (Bodenhausen and Ruben 1980) (acquisition times $t_1 = 0$, $t_2 = 122$ ms), the ^{1}H spectral width was 8,000 Hz and 977 points were collected. Ideal ^{1}H and ^{15}N pulses were employed, and dipole–dipole relaxation effects between spins were included, using correlation times of 8 ns for free Mms2 (145 residues) and 13 ns for Mms2 bound to Ub (total of 221 residues). The chemical shift of W33 $^{1}H_{\varepsilon 1}$ in the free state was set to 9.909 ppm (5,945.4 Hz), and 10.159 ppm (6,095.4 Hz) in the Ub-bound state. Post-acquisition processing included application of a cosine window function with a cutoff at 99 % of the length of the FID, and zero filling to 2,048 points. To simulate the effects of exchange between the free and Ub-bound states of Mms2, a K_D value of 300 μM with a $k_{off} = 2{,}500$ s^{-1} was used, as well as the protein and ligand concentrations listed in Tables 1 and 2. The fractional populations of free (p_A) and bound (p_B) protein (Mms2), for Methods 1 and 2 were calculated according to:

$$p_A = \frac{-K_D - L_T + P_T + \sqrt{K_D^2 + (L_T - P_T)^2 + 2K_D(L_T + P_T)}}{2P_T} \quad (8)$$

$$p_B = 1 - p_A \quad (9)$$

where P_T and L_T are the total protein and ligand concentrations, respectively. The free ligand concentration for the pseudo first order rate constant k_{on}[L] (Eq. 1) was calculated according to $k_{on} = k_{off}/K_D$ using:

$$[\mathrm{L}] = \frac{1}{2}\left[-K_D + L_T - P_T + \sqrt{K_D^2 + (L_T - P_T)^2 + 2K_D(L_T + P_T)}\right] \quad (10)$$

To assess the range of validity of line shape analysis, we also carried out GAMMA simulations for Methods 1 and 2 using the protein and ligand concentrations in Tables 1 and 2, with k_{off} values of 1,500 and 15,000 s^{-1} and respective K_D values of 180 and 1,800 μM. We also assessed the accuracy of a traditional titration (constant P_T) for k_{off} values of 1,500 and 15,000 s^{-1} and where the protein concentration is held at 0.5 mM, whereas the ligand concentration is varied according to values given in Table 1. To assess the impact of unresolved and partially resolved $^{1}H^{N}$–$^{1}H_{\alpha}$ ^{3}J couplings on the accuracy of line shape analysis, three GAMMA simulations were conducted using ligand concentrations as described in Table 1 for Method 1 and the protein concentration fixed at 0.5 mM, with the amide proton weakly coupled to a spin-1/2 nucleus with J values of 1.8, 5, and 10 Hz.

GAMMA simulations for ^{15}N were designed to produce similar, not identical, spectra to those experimentally observed for the main chain ^{15}N from T49 in human Mms2 upon titration with human Ub (Markin and Spyracopoulos 2012). A three spins-1/2 system was used, which included the scalar coupled main chain ^{15}N–$^{1}H^{N}$ pair (^{1}J set to 93 Hz), and the main chain $^{1}H_{\alpha}$. One-dimensional ^{15}N NMR spectra at a magnetic field strength of 14.1 Tesla (^{1}H Larmor frequency of 600 MHz) were simulated with the OverBodenhausen pulse sequence (acquisition time $t_1 = 118.6$ ms), the ^{15}N spectral width was 2,428.42 Hz and 288 points were collected. As in the case of simulated ^{1}H spectra, ideal ^{1}H and ^{15}N pulses were employed, and dipole–dipole relaxation effects between spins were

Table 1 Protein and ligand concentrations for GAMMA simulations of Method 1

Method 1, $k_{off} = 2{,}500$ s^{-1}, $K_D = 300$ μM						
$[P_T]$[a] (mM)	0.33	0.28	0.23	0.19	0.15	0.06
$[L_T]$[b] (mM)	0.0	0.18	0.39	0.56	0.71	1.06
p_A^c	1	0.738	0.518	0.402	0.330	0.228
p_B^d	0	0.262	0.482	0.598	0.670	0.772
k_{on}[L][e] (s^{-1})	0	888.3	2,326.2	3,719.8	5,079.0	8,447.5

[a] Total concentration of protein (Mms2)

[b] Total concentration of ligand (Ub)

[c] Population of free Mms2

[d] Population of Mms2 bound to Ub

[e] [L] is the free ligand, or Ub concentration, $k_{on} = 8.33 \times 10^{6}$ M^{-1} s^{-1}

Table 2 Protein and ligand concentrations for GAMMA simulations of Method 2

Method 2, $k_{off} = 2{,}500\ s^{-1}$, $K_D = 300\ \mu M$						
$[P_T]^a$ (mM)	0.44	0.59	0.49	0.39	0.29	0.20
$[L_T]^b$ (mM)	0	1.0	0.83	0.67	0.5	0.33
p_A^c	1	0.331	0.366	0.406	0.465	0.555
p_B^d	0	0.669	0.634	0.594	0.535	0.445
$k_{on}[L]^e$ (s^{-1})	0	5,045.6	4,328.3	3,653.7	2,874.2	2,007.7

[a] Total concentration of protein (Mms2)

[b] Total concentration of ligand (Ub)

[c] Population of free Mms2

[d] Population of Mms2 bound to Ub

[e] [L] is the free ligand, or Ub concentration, $k_{on} = 8.33 \times 10^6\ M^{-1}\ s^{-1}$

included, using correlation times of 8 ns for free Mms2 (145 residues) and 13 ns for Mms2 bound to Ub (total of 221 residues). The chemical shift of T49 ^{15}N in the free state was set to 122.53 ppm (7,479.73 Hz), and 120.0 ppm (7,325.29 Hz) in the Ub-bound state. Post-acquisition processing included application of a cosine window function with a cutoff at 99 % of the length of the FID, and zero filling to 1,024 points. The effects of exchange between free and Ub-bound states of Mms2 for Methods 1 and 2 were simulated using a K_D value of 300 μM with $k_{off} = 2{,}500\ s^{-1}$, and the Mms2 and Ub concentrations listed in Tables 1 and 2.

To test the range of validity of ^{15}N line shape analysis, we also carried out GAMMA simulations using Methods 1 and 2, with the protein and ligand concentrations in Tables 1 and 2, and k_{off} values of 100, 500, 1,000, and 15,000 s^{-1}, with respective K_D values of 12, 60, 120, and 1,800 μM. We also assessed the accuracy of traditional titrations that is, P_T held at 0.5 mM, for k_{off} values of 5, 500, 1,000 and 15,000 s^{-1} with respective K_D values of 0.6, 60, 120, and 1,800 μM, and where the ligand concentration is varied according to values given in Table 1.

Experimental NMR-monitored titrations

In this study, we applied classical line shape analysis on previous 2D ^1H–^{15}N HSQC NMR-monitored titrations of human Ub into [*U*-^{15}N]-Mms2 conducted using our recently developed chemical shift titrations (Methods 1 and 2) (Markin and Spyracopoulos 2012). Details regarding sample preparation, protein (Mms2) and ligand (Ub) concentrations, NMR data acquisition, and spectral processing are the same as previously reported (Markin and Spyracopoulos 2012), with the exception that the ^{15}N dimension for the chemical shift titrations was extended by linear prediction to a total of 384 points, multiplied by a 90°—shifted sine window, and zero filled to 1,024 points.

NMR line shape analyses for experimental and simulated NMR-monitored chemical shift titrations

In general, line shape analyses for simulated and experimental 2D ^1H–^{15}N HSQC NMR-monitored titrations were conducted using the Bloch-McConnell equations, modified to account for the application of time-domain apodization functions, within the program *Mathematica* 8.0.4. The detailed protocol for line shape analysis is as follows: analytical expressions for the frequency domain NMR spectra in the presence of exchange between the free and bound states were obtained from the Fourier transforms of the sum of the FIDs given by eqs. 2–7, after multiplication by sine time-domain window functions:

$$F(\omega) = M_0 \int_0^{t_{max}} \sin\left(n\pi + \frac{c\,\pi(1-n)t}{t_{max}}\right)^m (a_{11}(t) + a_{12}(t) + a_{22}(t) + a_{21}(t)) \exp(-i\,\omega\, t) dt \quad (11)$$

where n gives the shift in the time axis from a sine function ($n = 0$) to a cosine function ($n = 0.5$), c is the fractional cut-off in the time axis (typically 0.99), $m = 1$ (sine) or 2 (sine-squared), t_{max} is the acquisition time, and M_0 is a parameter to scale the arbitrary intensity of the frequency domain spectrum. For simulations of $^1H^N$ spectra using the Bloch-McConnell equations, in the presence of $^3J_{HNH\alpha}$ couplings, the spectrum can be assumed to be a weighted superposition of two uncoupled spectra corresponding to the upfield and downfield multiplet components, to a first approximation (Schmitt et al. 1995):

$$F_J(\omega) = \frac{1}{2}\left[F_{+J/2}(\omega) + F_{-J/2}(\omega)\right] \quad (12)$$

where $F_{+J/2}(\omega)$ and $F_{-J/2}(\omega)$ are the J-coupled multiplet components for the free and bound protein resonances. Thus, eqs. 2–7 are modified such that a spectrum with the free and bound resonance frequencies Ω_A, Ω_B is

represented by the weighted sum of two spectra at free and bound frequencies of $\Omega_A + \pi J$, $\Omega_B + \pi J$ and $\Omega_A - \pi J$, $\Omega_B - \pi J$.

One-dimensional traces from the proton dimension for the W33 indole side chain $^1H_{\varepsilon 1}$, and from the nitrogen dimension for the main chain amide for T49 were taken from the series of 2D ^{1}H–^{15}N HSQC NMR spectra acquired for the chemical shift titrations conducted using Methods 1 and 2. For each combination of free and bound protein populations (Tables 1, 2), traces were multiplied by their respective normalized protein concentrations, relative to the titration point with the most concentrated protein. In addition, each trace was multiplied by a factor to correct for differences in the number of transients collected relative to the spectrum with the fewest number of transients ($nt = 8$ or 16), that is, the respective factors were $8/nt$ or $16/nt$ for traces where $nt > 8$ or 16. In addition to these corrections, Eq. 11 is multiplied by a parameter for the overall intensity (M_0), whose value and that of the intrinsic transverse relaxation rate (R^0_{2A}), are derived from fits to Eq. 11 with $p_A = 1$, using the trace taken from the spectrum of free protein prior to line shape fitting of the entire titration. Note that $M_A(0)$ and $M_B(0)$ are set to 1 in eq. 11. The intrinsic transverse relaxation rate for the fully bound state, R^0_{2B}, was taken to be linearly dependent on the molecular mass increase for the bound state in comparison to the free state, that is, $R^0_{2B} = 1.5 \times R^0_{2A}$.

The preliminary steps described above yield traces from the individual NMR spectra of the chemical shift titrations with intensities corrected to match the following: an arbitrary experimental intensity factor, the concentration of the observed protein component, and the number of transients collected per titration point. Subsequently, traces are subjected to global minimization of the following objective function:

$$\chi\left(\Omega_B, k_{off}, h_{k>1}\right)^2 = \sum_{k=1}^{N}\sum_{l=1}^{np}\frac{\left(h_k F^k_{calc}(\omega_l) - F^k_{obs}(\omega_l)\right)^2}{\sigma_k^2} \tag{13}$$

where k is the kth NMR spectral trace from the kth titration point from the total N calculated (F_{calc}) or observed (F_{obs}) NMR spectra, with corresponding protein and ligand concentrations, l is the lth frequency point from the total np number of points of the calculated (F_{calc}) or observed (F_{obs}) kth NMR trace, and σ_k is the baseline noise from the kth NMR spectral trace from the kth titration point. The adjustable parameters in the objective function include the chemical shift for the bound state of the observed protein component (Ω_B), the off-rate of the protein–ligand interaction (k_{off}), and parameters ($h_{k>1}$) to optimize the calculated intensity of the kth trace, with the exception of the first trace, for which $h_1 = 1$. This trace corresponds to the free state of the observed protein; the arbitrary intensity of this trace is determined prior to line shape analysis through optimization of M_0, as described above. The remaining intensity parameters ($h_{k>1}$), are individually optimized for the k individual NMR traces. The individual optimization of intensity parameters has been demonstrated to correct for differential intensity losses, in comparison to the free state, between 2D ^{1}H–^{15}N HSQC spectra for different titration points as a result of relaxation and exchange in the dimension other than that being used for line shape analysis, as well as differential relaxation losses during INEPT polarization transfers (Günther and Schaffhausen 2002; Tugarinov and Kay 2003). For the calculated NMR traces (F_{calc}) in the objective function, k_{ex} (eqs. 3–7, $k_{ex} = k_{on}[\mathrm{L}] + k_{off}$) is given by:

$$k_{ex} = \frac{k_{off}}{2K_D}\left(K_D + L_T - P_T + \sqrt{(P_T + K_D)^2 + 2(K_D - P_T)L_T + L_T^2}\right) \tag{14}$$

Thus, K_D, L_T, and P_T are fixed at values determined from the experimental or theoretical design of the chosen chemical shift titration method, leaving k_{off} as an adjustable parameter. Finally, the chemical shift for the free state of the observed protein is fixed at the experimentally observed, or theoretically chosen value (Ω_A). Following optimization of M_0 and R^0_{2A} from the individual trace corresponding to the free state ($k = 1$), the objective function (Eq. 13) was subjected to nonlinear least squares regression in *Mathematica* 8.0.4 with the default parameters for the "NMinimize" and "Differential Evolution" options, with the fitted parameters k_{off}, Ω_B, and five intensity parameters (h_k) corresponding to the $k = 2, 3, 4, 5, 6$ (five total) different NMR traces collected in the presence of ligand. The first h_k intensity parameter for $k = 1$ is set to 1 and not optimized, as described above.

In general, for 1:1 protein–ligand interactions in the fast exchange regime, the K_D value used in line shape analyses is determined separately through non-linear least squares fits of chemical shift changes during the course of a titration, to a 1:1 binding isotherm. Therefore, in order to assess the impact of potential systematic errors in fitted K_Ds on the accuracy of line shape analyses, we determined K_D values from fits of the chemical shift changes observed in the ^{1}H and ^{15}N GAMMA simulations. These theoretical titrations were conducted using Methods 1 and 2 with the protein and ligand concentrations in Tables 1 and 2, and a traditional titration, that is, Method 1 with $P_T = 0.5$ mM, k_{off} values of 100, 500, 1,000, 2,500, and 15,000 s^{-1} for ^{15}N and k_{off} values of 1,500, 2,500, and 15,000 s^{-1} for ^{1}H. The chemical shifts of the resonances observed in the GAMMA simulations of the various titrations were

determined by fits to the natural NMR, or Lorentzian, line shape function:

$$I(v) = \frac{2M_0 R_2}{\pi\left(4(v - v_0)^2 + R_2^2\right)} \quad (15)$$

where the fitted parameters are M_0, an arbitrary intensity parameter, R_2, the transverse relaxation rate, and v_0, the chemical shift of the observed resonance. Chemical shifts for the various titrations with respective k_{off} values were fit to 1:1 binding isotherms to extract K_D values, as previously described (Markin and Spyracopoulos 2012). Errors in the fitted K_D values were determined using Monte Carlo methods by adding noise to the FIDs simulated with GAMMA, and choosing protein and ligand concentrations randomly from normal distributions as described in the following section.

Monte Carlo error estimation for NMR line shape analyses of simulated and experimental titrations

The errors associated with line shape analyses using the Bloch-McConnell equations for simulated and experimental ^{1}H–^{15}N HSQC NMR-monitored titrations were determined using Monte Carlo methods. For experimental titrations, and those simulated with the program GAMMA, we assumed that the two main sources of experimental error are the thermal electromotive force (EMF, or noise) in the probe coil, and the error in the starting protein and ligand concentrations. To generate an ensemble of 100 Monte Carlo titration data sets, that is, 600 NMR slices with corresponding protein:ligand ratios used in experimental titrations or those for GAMMA NMR simulations of Methods 1 and 2 (Tables 1, 2), random noise was added to each point of an FID corresponding to a single NMR slice at a given protein:ligand ratio. For the experimental titrations, theoretical FIDs were calculated from the Bloch-McConnell equations, using the fitted parameters determined from line shape analysis, and noise was added to these back-calculated FIDs. The magnitude of the noise for a given FID was empirically adjusted such that the signal to noise ratio after Fourier transformation and post acquisition processing matched that observed experimentally for the NMR slice corresponding to the free state. In addition, the initial protein and ligand concentrations were chosen randomly from a normal distribution with a standard deviation of 5 %, and subsequent concentrations were calculated according to the respective dilution factor, as previously discussed (Markin and Spyracopoulos 2012). For titrations conducted through addition of a single stock solution of ligand (Method 1), by dilution (Method 2), or both, the maximum concentration error involves only the starting concentrations of protein and ligand, as subsequent errors due to pipetting and or dilution are small (Markin and Spyracopoulos 2012). The ensemble of 100 Monte Carlo titration data sets were fit to the Bloch-McConnell equations as described in the previous section, and statistics for the resulting χ^2, k_{off}, and bound chemical shift (Ω_B) ensembles were calculated.

Results and discussion

Accuracy of kinetic parameters from NMR-monitored chemical shift titrations

Careful experimental design of 2D ^{1}H–^{15}N NMR-monitored titrations for the study of protein–ligand interactions has the potential to produce a wealth of information regarding thermodynamic parameters such as dissociation constants (K_D) and concomitant populations for the free and bound states, obtainable through chemical shift analyses, as well as the kinetics of exchange between states, which can be determined through line shape analyses.

We recently developed precise 2D ^{1}H–^{15}N NMR-monitored chemical shift titration methods for the determination of protein–ligand K_D values with kinetics in the fast exchange regime on the NMR timescale (Markin and Spyracopoulos 2012). The key to greater accuracy and precision with respect to the determination of K_D using these methods is the co-variation of the protein and ligand concentrations during the course of an NMR-monitored titration. One method entails the addition of aliquots of concentrated ligand solution to a concentrated protein solution, wherein the protein concentration decreases by a constant factor (Method 1), or alternatively, sequential dilution of a solution of concentrated protein and ligand in an initial 1:2 ratio (Method 2). This latter method yields fairly robust precision over a broad range of K_D values. It is of interest therefore, to determine if classical line shape analysis applied to these chemical shift titration methods can give accurate and precise off-rates for a given protein–ligand interaction.

The first issues to address are generalizations that line shape analyses are rarely practical for large proteins, and that limited digital resolution in heteronuclear 2D NMR spectroscopy may lead to inaccurate kinetics (Palmer et al. 2001; Lian and Roberts 2011). Using the GAMMA program (Smith et al. 1994), we performed quantum mechanical NMR simulations of the chemical shift titration experiments we developed, in order to assess the impact of digital resolution and post-acquisition processing on the accuracy of kinetic parameters derived from classical line shape analyses. The agreement between titrations simulated with the GAMMA program, and the associated fits to the Bloch-McConnell equations is excellent, as shown in

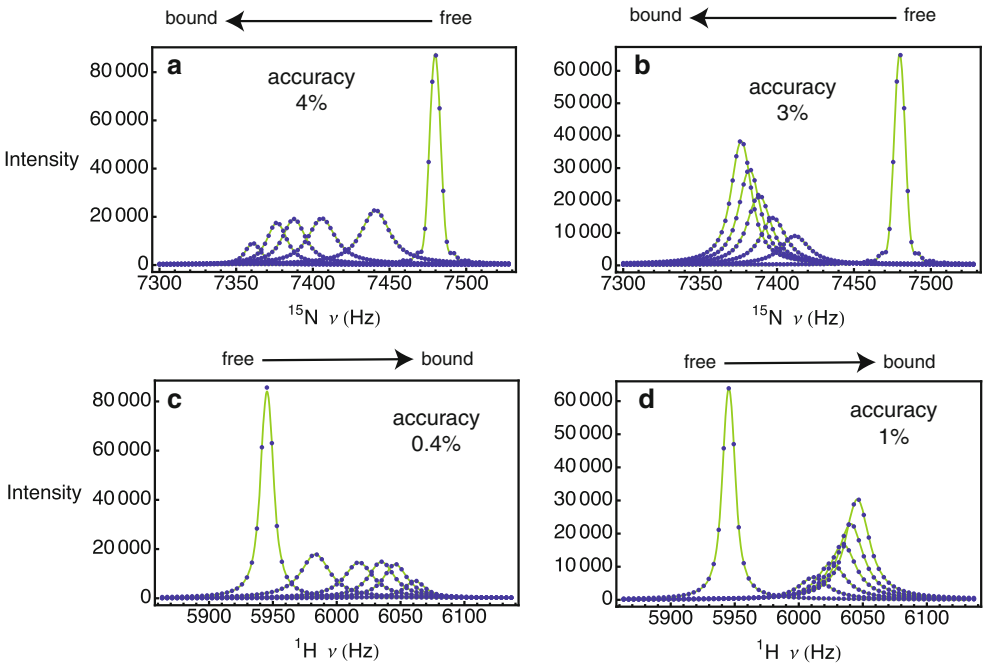

Fig. 1 GAMMA simulations for **a** T49 ^{15}N Method 1 (*blue circles*), with corresponding fits to the Bloch-McConnell equations (*green lines*), **b** T49 ^{15}N for Method 2, **c** W33 $^{1}H_{\varepsilon 1}$ for Method 1, and **d** ^{1}H for Method 2. The accuracy of the fitted k_{off} is given in the individual figure panels

Table 3 Line shape analysis for Methods 1 and 2 simulated with GAMMA

	$\chi^2 \times 10^8$	k_{off} (s^{-1})	ν_B (Hz)	$M_0^a \times 10^6$	$R_{2A}^{0\,a}$ (s^{-1})	h_2	h_3	h_4	h_5	h_6
M1[b], ^{15}N	0.315	2,390.27	7,325.99	1.815	11.807	1.032	1.033	1.039	1.028	1.026
M2[c], ^{15}N	3.053	2,432.61	7,325.91	1.815	11.809	1.024	1.024	1.025	1.026	1.028
M1, ^{1}H	0.069	2,509.93	6,095.33	2.954	30.135	0.517	0.425	0.387	0.330	0.147
M2, ^{1}H	0.031	2,484.94	6,095.43	2.949	29.327	0.721	0.689	0.668	0.633	0.598

[a] M_0 and R_{2A}^0 were optimized separately from the line shape analysis using the NMR trace corresponding to the free state

[b] M1 indicates Method 1

[c] M2 indicates Method 2

Fig. 1 and Table 3. For ^{15}N, with $k_{off} = 2{,}500\ s^{-1}$ and $K_D = 300\ \mu M$, the absolute difference between the actual and fitted k_{off} is 4.4 and 2.7 % for Methods 1 and 2, respectively, and the absolute difference between the actual and fitted $\Delta\omega$ is 1.3 % for both Methods 1 and 2 (Fig. 1 and Table 3). For the ^{1}H dimension, with $k_{off} = 2{,}500\ s^{-1}$ and $K_D = 300\ \mu M$, the absolute difference between the actual and fitted k_{off} is 0.4 and 0.6 % for Methods 1 and 2, respectively, and the absolute difference between the actual and fitted $\Delta\omega$ is 0.15 and 0.02 % for Methods 1 and 2, respectively (Fig. 1 and Table 3).

The excellent accuracy of classical line shape analysis underscores a number of key points: First, the digital resolution of typical 2D ^{1}H–^{15}N HSQC NMR spectra (^{1}H: 8.2 Hz/point, ^{15}N: 12.6 Hz/point) does not appear to seriously impede the accuracy of line shape analysis when typical post-acquisition processing techniques such as multiplication of FIDs by cosine apodization functions, zero-filling (^{1}H and ^{15}N dimensions), and linear prediction (^{15}N dimension) are employed. Secondly, in the absence of spin–spin couplings, the Bloch–McConnell equations, that is, the equations of motion for nuclear spins undergoing chemical exchange derived using classical physics, are essentially identical to those derived using a quantum mechanical approach, as expected (Bain 2003). Third, optimization of individual intensity parameters for respective ^{1}H and ^{15}N traces taken from individual spectra for various titration points is an effective approach to account for differential relaxation and exchange losses during INEPT transfers and acquisition of two dimensions, as previously pointed out (Günther and Schaffhausen 2002; Tugarinov and Kay 2003). Finally, fitting the line shape of the free state to the Bloch-McConnell equations with $p_A = 1$ (Eq. 11) is a reasonable approach to estimate the

Table 4 Experimental line shape analysis for Methods 1 and 2

	χ^2	k_{off} (s^{-1})	ν_B (Hz)	$M_0^a \times 10^6$	$R_{2A}^{0\,a}$ (s^{-1})	h_2	h_3	h_4	h_5	h_6
M1[b], ^{15}N	170.684	3,004.11	7,333.60	1.724	20.515	0.843	0.666	0.652	0.607	0.527
M2[c], ^{15}N	305.679	3,633.51	7,321.41	3.706	19.714	0.920	0.911	0.904	0.872	0.854
M1, ^{1}H	33.530	3,568.74	6,080.97	1.303	48.089	0.634	0.564	0.557	0.558	0.560
M2, ^{1}H	55.548	3,179.61	6,088.84	2.654	41.313	0.873	0.841	0.735	0.782	0.729

[a] M_0 and R_{2A}^0 were optimized separately from the line shape analysis using the NMR trace corresponding to the free state

[b] M1 indicates Method 1

[c] M2 indicates Method 2

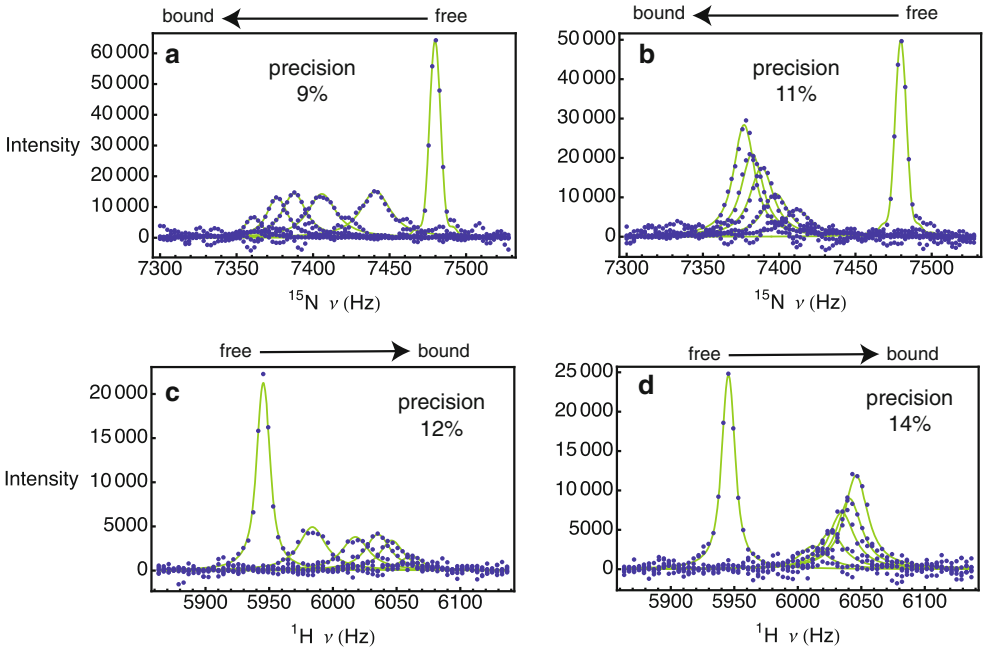

Fig. 2 **a** One dimensional ^{15}N traces taken through the cross-peaks of T49 from 2D ^{1}H–^{15}N HSQC NMR spectra for Method 1 (*blue circles*), with corresponding fits to the Bloch-McConnell equations (*green lines*), and **b** ^{15}N traces taken through the cross-peaks of T49 for Method 2. **c** One dimensional $^{1}H_{\varepsilon 1}$ traces taken through the cross-peaks of the W33 from 2D ^{1}H–^{15}N HSQC NMR spectra for Method 1 (*blue*), with corresponding fits to the Bloch-McConnell equations (*green lines*), and **d** $^{1}H_{\varepsilon 1}$ traces for Method 2. The precision of the fitted k_{off} is given in the individual figure panels

intrinsic transverse relaxation rate R_{2A}^0. For example, using the three spins-1/2 system described in the Theory and Methods section, the calculated T49 ^{15}N dipole–dipole transverse relaxation rate from GAMMA is 11.4 s^{-1}, and the average fitted value is 11.8 s^{-1} for Methods 1 and 2 (Table 3). For the five spins-1/2 system (Theory and Methods), the calculated W33 $^{1}H_{\varepsilon 1}$ dipole–dipole transverse relaxation rate from GAMMA is 25.4 s^{-1}, and the average fitted value is 29.7 s^{-1} for Methods 1 and 2 (Table 3).

Experimentally, the average k_{off} value determined for the Mms2–Ub interaction using classical line shape analysis for Methods 1 and 2 is 3,347 s^{-1} for T49 ^{15}N and W33 $^{1}H_{\varepsilon 1}$ (Table 4 and Fig. 2). The standard deviation in the mean value is 304 s^{-1}, or 9 %. Thus, the excellent agreement for k_{off} between two separate chemical shift titrations (Methods 1 and 2), and different nuclei from two residues, is consistent with the precision of classical line shape analysis as implemented in Methods 1 and 2, as discussed in detail in the subsequent section.

Precision of kinetic parameters from NMR-monitored chemical shift titrations

In the previous section, it was demonstrated that classical line shape analysis is highly accurate (<5 %) for chemical shift titration methods we recently developed. To estimate the precision of kinetic parameters derived from classical line shape analyses in the presence of experimental noise and random error, we conducted Monte Carlo trials for

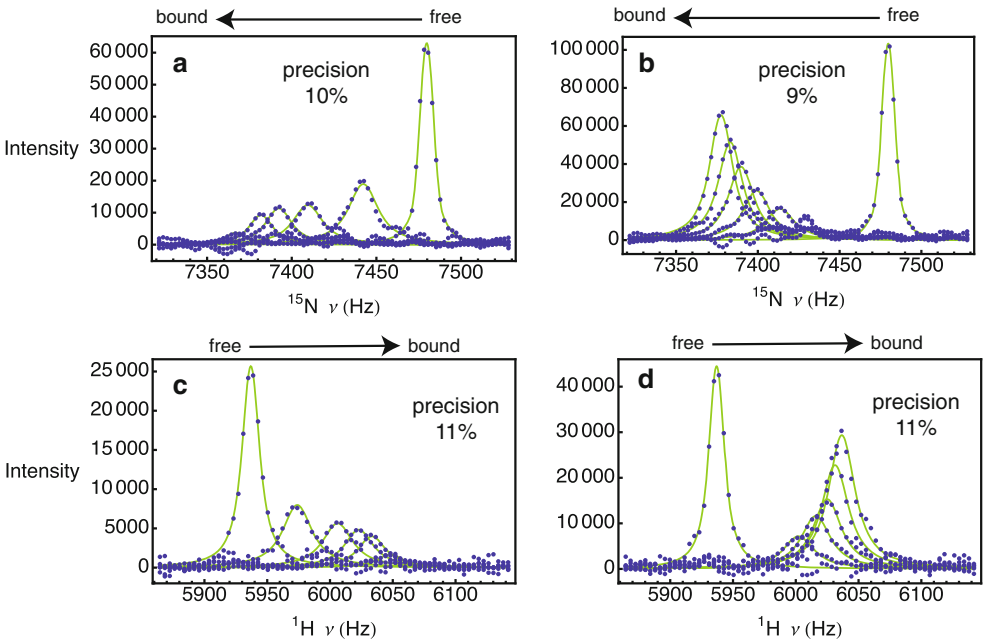

Fig. 3 GAMMA simulations in the presence of noise and concentration error for (**a**) T49 ^{15}N Method 1 (*blue circles*), with corresponding fits to the Bloch-McConnell equations (*green lines*), (**b**) T49 ^{15}N for Method 2, (**c**) W33 $^{1}H_{\varepsilon 1}$ for Method 1, and (**d**) W33 $^{1}H_{\varepsilon 1}$ for Method 2. The precision of the fitted k_{off} is given in the individual figure panels

Table 5 Errors for line shape analysis for Methods 1 and 2 simulated with GAMMA

	χ^2	k_{off} (s^{-1})	ν_B (Hz)
M1[a], ^{15}N	295 ± 43	2,421 ± 223 (9 %)[b]	7,326 ± 3 (0.04 %)[c]
M2[d], ^{15}N	347 ± 38	2,625 ± 286 (11 %)	7,326 ± 4 (0.05 %)
M1, ^{1}H	164 ± 19	2,780 ± 298 (12 %)	6,096 ± 3 (0.05 %)
M2, ^{1}H	850 ± 69	2,795 ± 347 (14 %)	6,096 ± 4 (0.07 %)

[a] M1 indicates Method 1

[b] The standard deviation as a percentage of the actual k_{off} (2,500 s^{-1}) is given in parentheses

[c] The standard deviation as a percentage of the actual ν_B (7,326 or 6,096 Hz) is given in parentheses

[d] M2 indicates Method 2

GAMMA simulations of chemical shift titrations using the experimental designs of Methods 1 and 2. We assumed that the two main sources of experimental error during an NMR-monitored titration arise from thermal EMF in the NMR probe coil due to the Brownian motion of electrons, ultimately manifested as noise in the spectrum (Hoult 1978), and the error in the starting concentrations of protein and ligand (Markin and Spyracopoulos 2012). Representative spectra for the various chemical shift titration methods in the presence of simulated thermal EMF that is similar in magnitude to that observed experimentally, as well as concentration errors, are shown in Fig. 3 and can be compared to the analogous spectra in the absence of noise (Fig. 1).

The average error in k_{off} for residues T49 (^{15}N) and W33 (^{1}H) determined using Monte Carlo parameter estimation for GAMMA NMR simulations of Methods 1 and 2 is 12 % (Table 5). Representative Monte Carlo ensembles for line shape analyses for T49 ^{15}N, Methods 1 and 2 are shown in Fig. 4. The average error in $\Delta\nu$, or $|\Omega_A - \Omega_B|/2\pi$, the maximum chemical shift change, for residues T49 (^{15}N) and W33 (^{1}H) determined using Monte Carlo parameter estimation for GAMMA NMR simulations of Methods 1 and 2 is 0.05 % (Table 5). The average parameter bias from Monte Carlo trials of the GAMMA simulations for Methods 1 and 2, that is, the difference between the mean of the ensemble of fitted parameters (k_{off} and ν_B) and their actual values is 8 % for k_{off}, and 0.4 % for ν_B. The parameter bias is within the error range from the Monte Carlo trials, indicating that the fitting procedure is of good quality, and free of systematic error.

The precision of GAMMA simulations in the presence of noise and concentration errors for Methods 1 and 2 is comparable to the experimentally determined precision. For example, the average error in k_{off} for residues T49 (^{15}N) and W33 (^{1}H) determined using Monte Carlo parameter estimation for Methods 1 and 2 is 10 % (Table 6). The average error in the experimentally determined $\Delta\nu$, the maximum chemical shift change, for residues T49 (^{15}N) and W33 (^{1}H) from Monte Carlo parameter estimation for Methods 1 and 2 is 0.06 % (Table 6). The parameter biases, the differences between the experimental means and the means of the Monte Carlo

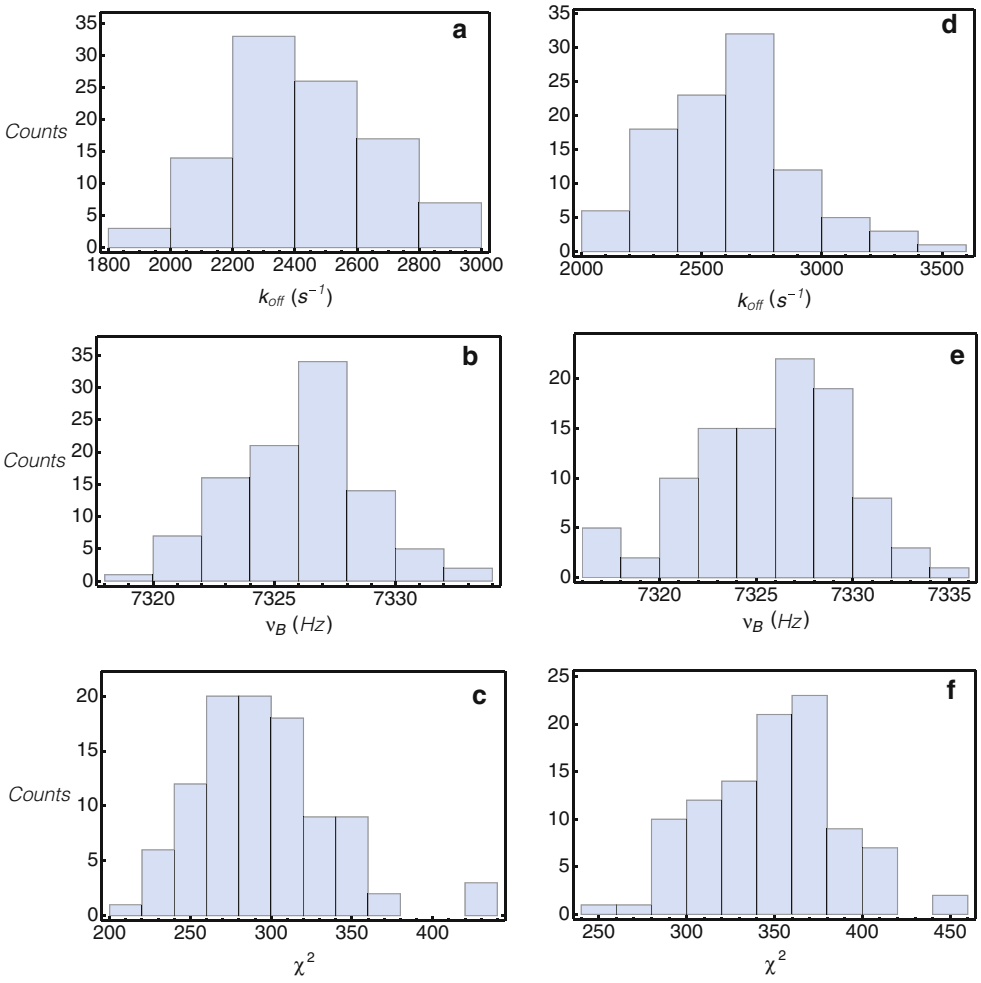

Fig. 4 Monte Carlo parameter ensembles for line shape analyses of T49 ^{15}N GAMMA simulations, Method 1: **a** k_{off}, **b** the bound chemical shift ν_B, and **c** the magnitude of the objective function after optimization, χ^2. Monte Carlo parameter ensembles for line shape analyses of T49 ^{15}N GAMMA simulations, Method 2: **d**k_{off}, **e** the bound chemical shift ν_B, and **f** the magnitude of the objective function after optimization, χ^2

Table 6 Errors for experimental line shape analysis for Methods 1 and 2

	χ^2	k_{off} (s^{-1})	ν_B (Hz)
M1[a], ^{15}N	242 ± 36	2,788 ± 293 (10 %)[b]	7,333 ± 3 (0.04 %)[c]
M2[d], ^{15}N	1,266 ± 107	3,364 ± 324 (9 %)	7,321 ± 5 (0.07 %)
M1, ^{1}H	216 ± 22	3,311 ± 409 (11 %)	6,081 ± 3 (0.05 %)
M2, ^{1}H	480 ± 47	3,078 ± 345 (11 %)	6,089 ± 4 (0.07 %)

[a] M1 indicates Method 1

[b] The standard deviation as a percentage of the fitted k_{off} in Table 4 is given in parentheses

[c] The standard deviation as a percentage of the fitted ν_B in Table 4 is given in parentheses

[d] M2 indicates Method 2

ensembles, for k_{off} and $\Delta\nu$ are 6 and 0.3 %, respectively, indicative of good quality fits lacking systematic errors. As previously noted, the mean of the experimental k_{off} has a value for $\pm 1\sigma$ of 9 %, indicating that our estimates for the magnitude of thermal EMF in the probe coil and the protein concentration errors are reasonable, and likely to properly account for the main sources of experimental error.

Theoretical range of validity for line shape analyses of NMR-monitored chemical shift titrations

In addition to GAMMA simulations conducted with a k_{off} value of 2,500 s^{-1}, we also conducted GAMMA simulations with k_{off} values of 500, 1,000 and 15,000 s^{-1} and $K_D = 60$, 120, and 1,800 μM, respectively, for T49 ^{15}N using Methods 1 and 2, as well as traditional NMR

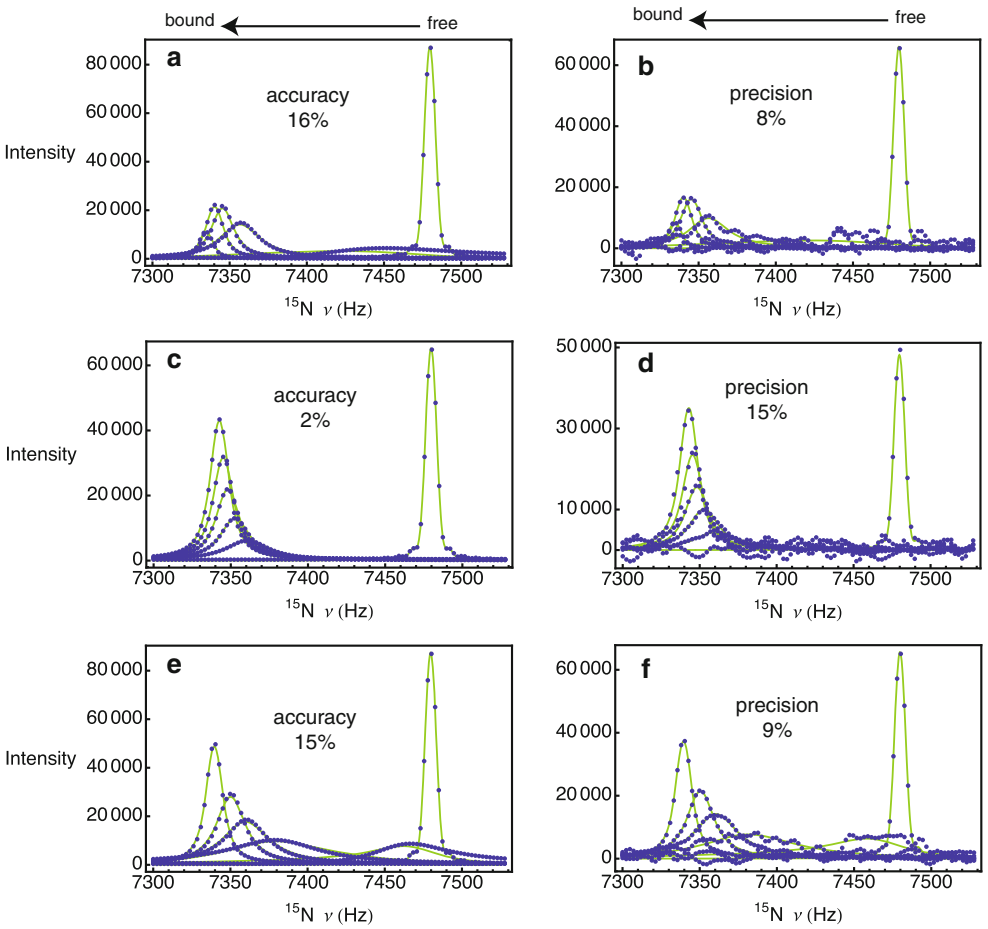

Fig. 5 GAMMA simulations for $K_D = 60$ μM and $k_{off} = 500$ s^{-1} using T49 ^{15}N Method 1 (*blue circles*), with corresponding fits to the Bloch-McConnell equations (*green lines*) in absence (**a**) and the presence (**b**) of noise and concentration error. ^{15}N Method 2 in the absence (**c**) and presence (**d**) of noise and concentration error. ^{15}N Method 1 with P_T fixed at 0.5 mM (traditional titration) in the absence (**e**) and presence (**f**) of noise and concentration error. The accuracy or precision of the fitted k_{off} is given in the individual figure panels

titrations, that is, Method 1 with P_T held constant at 0.5 mM (Figs. 5, 6, 7 and Table 7). These k_{off} values were chosen as they represent approximate, qualitative limits of applicability for line shape analysis for this specific protein–protein interaction. The lower k_{off} limit is determined by the amount of line broadening, and the resulting impact on signal to noise ratio (Fig. 6b, d, e). The upper k_{off} limit was chosen as it represents the approximate K_D value (1.8 mM) beyond which the biological relevance of an interaction becomes questionable.

For T49 ^{15}N, Method 2 yields the most accurate values for $k_{off} = 500$ and 1,000 s^{-1}, with absolute differences of 3 and 2 %, respectively, whereas Method 1 is substantially less accurate at 16 and 7 % for $k_{off} = 500$ and 1,000 s^{-1}, respectively (Figs. 5, 6). The traditional method for conducting a titration is also substantially less accurate than Method 2 at 15 and 8 % for $k_{off} = 500$ and 1,000 s^{-1}, respectively (Figs. 5, 6). This decrease in accuracy for Method 1 and traditional titrations is due to the fact that Method 2 has fewer points within the region of protein:ligand ratios that have substantial line broadening (compare Figs. 5c, 6c with Figs. 5a, 6a and 5e, 6e). In this exchange regime, for the first titration point with $k_{off} = 500$ s^{-1} (Fig. 5a, e), the free and bound resonances are differentially broadened, have different intensities, and are not averaged to a single resonance. This phenomenon is manifested as a single asymmetric peak in the spectrum. Furthermore, the agreement between spectra calculated using a quantum mechanical approach and the classical Bloch-McConnell equations is somewhat worse than at faster exchange rates with $k_{off} > 500$ s^{-1}, that is, the accuracy in k_{off} drops from ~8 % at $k_{off} = 1{,}000$ s^{-1} to ~16 % at $k_{off} = 500$ s^{-1}; compare the first titration points in Figs. 5a, 6a and 5e, 6e. This observation highlights the fact that the lower limit of exchange for which chemical shift titrations can be used to fit K_D values is determined by incomplete averaging of the free and bound peaks to a single resonance. In addition, given that Method 2 does not sample this region to the same extent as Method 1, or traditional titrations, Method 2 provides

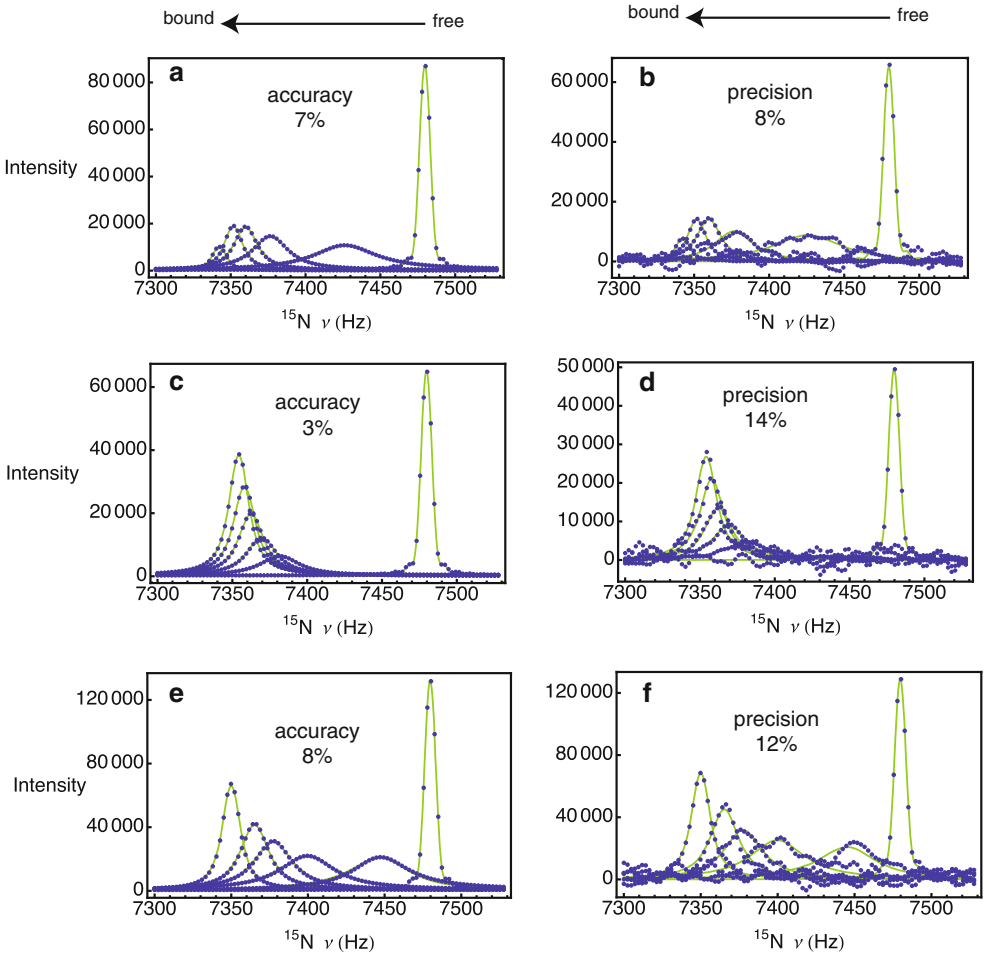

Fig. 6 GAMMA simulations for $K_D = 120$ μM and $k_{off} = 1{,}000$ s^{-1} using ^{15}N Method 1 (*blue circles*), with corresponding fits to the Bloch-McConnell equations (*green lines*) in absence (**a**) and the presence (**b**) of noise and concentration error. ^{15}N Method 2 in the absence (**c**) and presence (**d**) of noise and concentration error. ^{15}N Method 1 with P_T fixed at 0.5 mM (traditional titration) in the absence (**e**) and presence (**f**) of noise and concentration error. The accuracy or precision of the fitted k_{off} is given in the individual figure panels

a means to extend the limit of applicability of chemical shift titrations and line shape analyses to intermediate exchange rates; this is discussed in more detail below, and in subsequent sections.

In addition to analyzing accuracy, the precision for k_{off} determined from the various ^{15}N line shape methods was determined from statistical analyses of the ensembles of 100 Monte Carlo distributions. For Methods 1 and 2, with k_{off} values of 500 and 1,000 s^{-1}, the precision is reasonable (8–15 %) given a typical signal to noise ratio for the free peak of ~50:1, and an error in protein concentration of 5 % (Figs. 5b, d, f and 6b, d, f). For T49 ^{15}N within the very fast exchange regime, $k_{off} = 15{,}000$ s^{-1} (Fig. 7), line shape analysis for Methods 1 and 2, as well as a traditional titration with $P_T = 0.5$ mM, produces accurate values of k_{off}, within ~1 % (Fig. 7a, c, e). In addition, Monte Carlo simulations in the presence of noise and concentration error indicate that the precision is good, ~9–10 % for all three methods.

We conducted GAMMA simulations with k_{off} values of 1,500 and 15,000 s^{-1} and $K_D = 180$ and 1,800 μM, respectively, for W33 $^1H_{\varepsilon 1}$ using Methods 1 and 2, as well as Method 1 with P_T held at 0.5 mM (Figs. 8, 9, and Table 8). For the fast exchange regime $k_{off} = 1{,}500$ s^{-1}, the accuracy is better than 1 % for all of the titrations (Fig. 8a, c, e), with the precision ranging from 10 to 17 % (Fig. 8b, d, f). Within the very fast exchange regime, $k_{off} = 15{,}000$ s^{-1}, Method 2 reproduces k_{off} with the greatest accuracy (0.5 %, Fig. 9c), whereas Method 1, as well as a traditional titration with $P_T = 0.5$ mM, are substantially less accurate at 16 and 14 % (Fig. 9a, e), respectively. Regardless of the differences in accuracy, the precision for the various methods in the very fast exchange regime ranges from 10 to 17 % (Fig. 9b, d, f).

The theoretical analysis of the accuracy and precision of line shape analysis indicates that for a protein–protein interaction such as that between Mms2 (145 residues) and

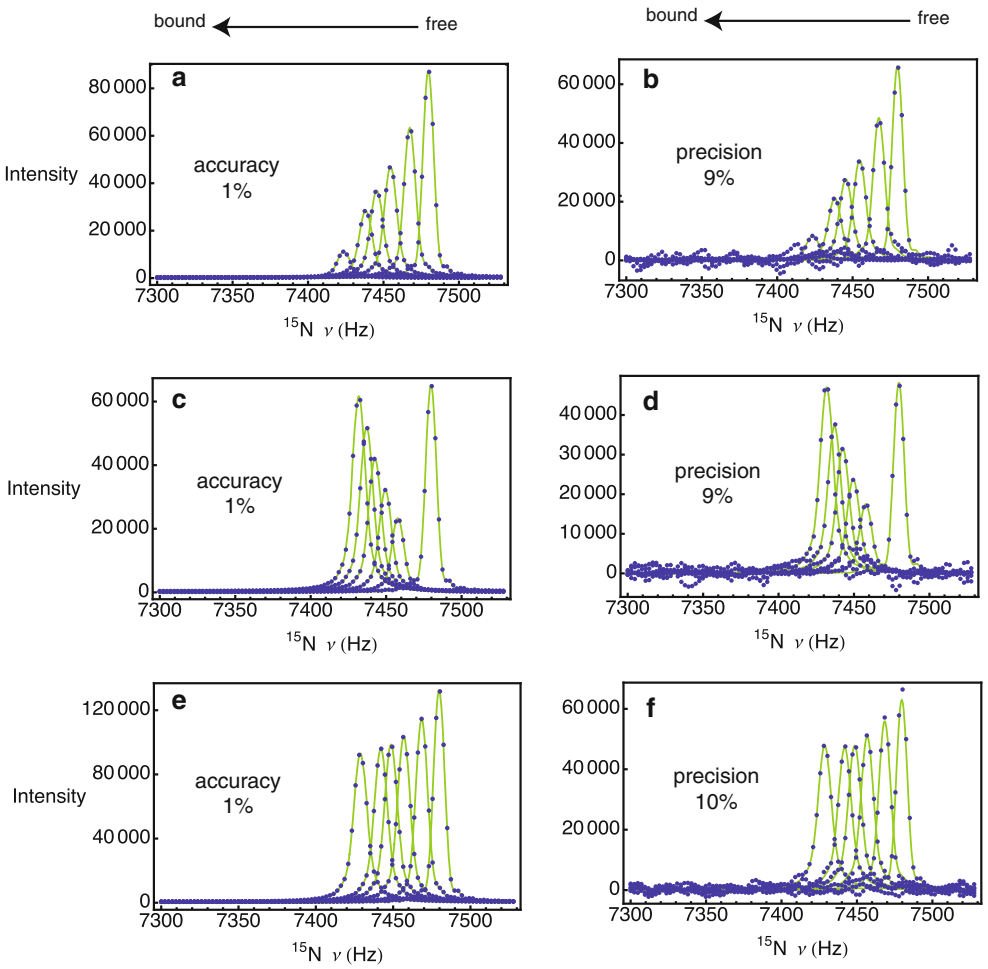

Fig. 7 GAMMA simulations for $K_D = 1{,}800$ μM and $k_{off} = 15{,}000$ s^{-1} using ^{15}N Method 1 (*blue circles*), with corresponding fits to the Bloch-McConnell equations (*green lines*) in absence (**a**) and the presence (**b**) of noise and concentration error. ^{15}N Method 2 in the absence (**c**) and presence (**d**) of noise and concentration error. ^{15}N Method 1 with P_T fixed at 0.5 mM (traditional titration) in the absence (**e**) and presence (**f**) of noise and concentration error. The accuracy or precision of the fitted k_{off} is given in the individual figure panels

Table 7 Theoretical Accuracy and Precision for ^{15}N Line Shape Analysis for Methods 1 and 2 Simulated with GAMMA

k_{off}	M1[a]	M2[b]	M1-trad[c]
100 s^{-1}	n.d.[d]	4 (±13) % [e]	n.d.
500 s^{-1}	16 (±8) % [e]	2 (±15) %	15 (±9) %
1,000 s^{-1}	7 (±8) %	3 (±14) %	8 (±12) %
15,000 s^{-1}	1 (±9) %	1 (±9) %	1 (±10) %

[a] M1 indicates Method 1 with protein and ligand concentrations in Table 1

[b] M2 indicates Method 2 with protein and ligand concentrations in Table 2

[c] M1-trad indicates Method 1, with P_T fixed at 0.5 mM and ligand concentrations in Table 1

[d] Not determined

[e] The precision calculated from the Monte Carlo ensemble is given in parentheses

ubiquitin (76 residues), with the specific acquisition parameters used in this study (Materials and Methods), line shape analysis using the ^{15}N dimension from 2D ^{1}H–^{15}N HSQC NMR spectra is accurate to better than 8 % and the precision better than 14 % for k_{off} ranging from 1,000 s^{-1} to 15,000 s^{-1} (Table 7). To assess an approximate lower limit for k_{off}, it is reasonable to assume that Method 2 is most likely to produce quantitative kinetics for intermediate exchange rates ($k_{off} < 1{,}000$ s^{-1}) where line broadening is extensive, as the experimental design avoids protein:ligand ratios that approach this regime. Therefore, we conducted simulations for ^{15}N with $k_{off} = 100$ s^{-1} (Fig. 10). From these results, it is evident that Method 2 in the ^{15}N dimension provides good accuracy and precision for k_{off}, better than 4 %, for values of 100 and 500 s^{-1} (Table 7 and Fig. 10). If the K_D value for a protein–protein or protein ligand interaction is below ~ 1 μM, isothermal titration calorimetry can be used to measure K_D, and

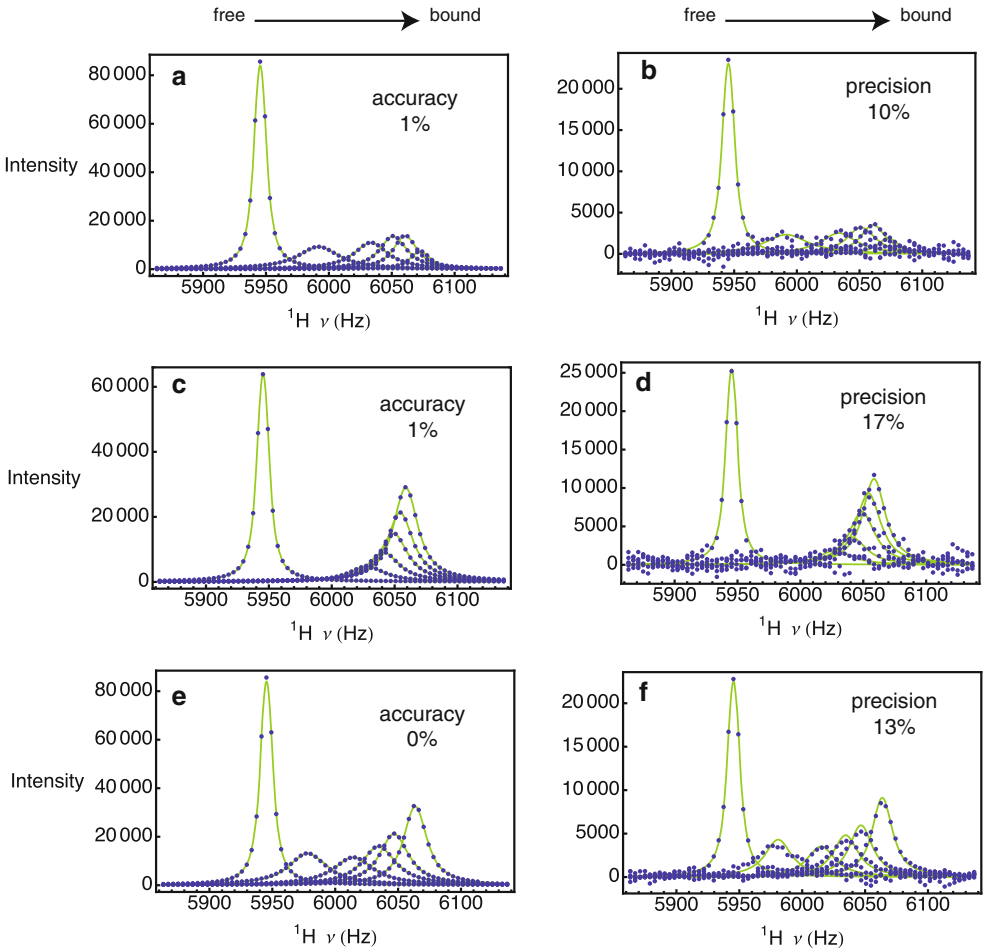

Fig. 8 GAMMA simulations for $K_D = 180$ μM and $k_{off} = 1{,}500$ s^{-1} using ^{1}H Method 1 (*blue circles*), with corresponding fits to the Bloch-McConnell equations (*green lines*) in absence (**a**) and the presence (**b**) of noise and concentration error. ^{1}H Method 2 in the absence (**c**) and presence (**d**) of noise and concentration error. ^{1}H Method 1 with P_T fixed at 0.5 mM (traditional titration) in the absence (**e**) and presence (**f**) of noise and concentration error. The accuracy or precision of the fitted k_{off} is given in the individual figure panels

therefore, can potentially extend the applicability of classical line shape analysis into the slow exchange limit (McKenna et al., 2003; Markin et al., 2010b). For example, from GAMMA simulations of a traditional titration, or Method 1 with P_T fixed at 0.5 mM, and ligand concentrations in Table 1, for ^{15}N with $k_{off} = 5$ s^{-1}, and $K_D = 0.6$ μM, the accuracy for k_{off} is 5 %, however, the precision is poor at ~30 % (Fig. 11).

Line shape analyses using the ^{1}H^N dimension yields accurate kinetics above ~ 1,500 s^{-1}; the agreement with the actual k_{off} is better than 1 %, with reasonable precision ranging from 10 to 17 %. Below this k_{off}, line broadening for protein:ligand ratios that are ~ 1:1 renders line shape analysis using data from the ^{1}H^N dimension difficult. At the biologically relevant upper limit, $k_{off} = 15{,}000$ s^{-1}, the accuracy is impaired (14–16 %) in comparison to the ^{15}N dimension for Method 1, as well as the traditional method of conducting a titration. However, the accuracy of 0.5 % for Method 2 at $k_{off} = 15{,}000$ s^{-1} remains comparable to that obtained in the ^{15}N dimension. Thus, for the protein–protein system and experimental parameters employed in this study, line shape analyses using ^{1}H–^{15}N HSQC 2D NMR monitored titrations have the potential to provide reasonably accurate and precise k_{off} values over a wide range, from 100 to 15,000 s^{-1}. Ultimately, the accuracy of k_{off} is subject to systematic errors arising from $^3J_{HNH\alpha}$ couplings, as well as the accuracy of K_D and R^0_{2A} employed in line shape analyses, as discussed in detail in subsequent sections.

Systematic errors in ^{1}H^N line shape analyses of NMR-monitored chemical shift titrations due to $^3J_{HNH\alpha}$ couplings

For typical 2D ^{1}H–^{15}N HSQC 2D NMR spectra of small to moderately sized proteins (10–30 kDa), per residue cross peaks from the ^{1}H^N dimension display partially resolved or

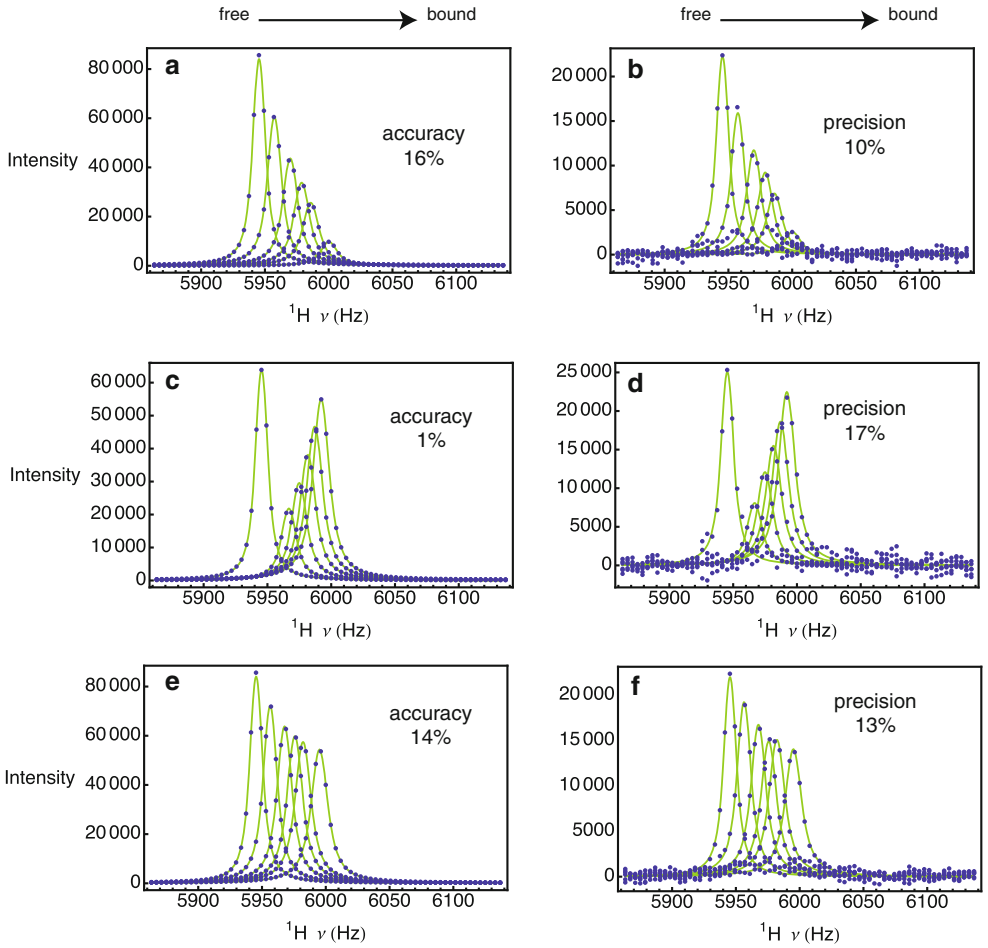

Fig. 9 GAMMA simulations for $K_D = 1{,}800$ μM and $k_{off} = 15{,}000$ s^{-1} using ^{1}H Method 1 (*blue circles*), with corresponding fits to the Bloch-McConnell equations (*green lines*) in absence (**a**) and the presence (**b**) of noise and concentration error. ^{1}H Method 2 in the absence (**c**) and presence (**d**) of noise and concentration error. ^{1}H Method 1 with P_T fixed at 0.5 mM (traditional titration) in the absence (**e**) and presence (**f**) of noise and concentration error. The accuracy or precision of the fitted k_{off} is given in the individual figure panels

Table 8 Theoretical accuracy and precision for ^{1}H line shape analysis for Methods 1 and 2 simulated with GAMMA

k_{off} (s^{-1})	M1[a]	M2[b]	M1-trad[c]
1,500	1 (±10) %[d]	1 (±17) %	0 (±13) %
15,000	16 (±10) %	1 (±17) %	14 (±13) %

[a] M1 indicates Method 1 with protein and ligand concentrations in Table 1

[b] M2 indicates Method 2 with protein and ligand concentrations in Table 2

[c] M1-trad indicates Method 1, with P_T fixed at 0.5 mM and ligand concentrations in Table 1

[d] The precision calculated from the Monte Carlo ensemble is given in parentheses

unresolved coupling to the respective $^1H_\alpha$ of a given residue ($^3J_{HNH\alpha}$). The magnitude of the coupling is dependent on the main chain ϕ dihedral angle, according to the Karplus equation, and ranges from ~4 Hz for α-helical secondary structure, ~7 Hz for averaged random coil configurations, and ~10 Hz for β-sheet conformations (Cavanagh 2007). If the phenomenological Bloch equations are employed to analyze kinetic processes using NMR line shape analysis, unresolved $^3J_{HNH\alpha}$ couplings typically cannot be ignored, as the resulting kinetics may be inaccurate. For example, Fig. 12 shows the accuracy of $^1H^N$ line shape analysis in the presence of unresolved or partially resolved $^3J_{HNH\alpha}$ couplings. For GAMMA simulations of Method 1 (Table 1, $k_{off} = 2{,}500$ s^{-1}) with an unresolved $^3J_{HNH\alpha}$ of 1.8 Hz for a $^1H^N$ resonance peak with an intrinsic R_2^0 of 25 s^{-1}, an acquisition time of 122 ms, a digital resolution of 8.2 Hz/point, and post-acquisition processing of the FID by a cosine window function and zero-filling to 2,048 points, the k_{off} is reproduced with an accuracy of 0.4 % (Fig. 12a). This indicates that couplings below 2 Hz can be ignored in line shape analyses when employing the Bloch equations at the spectral resolution employed in this work. It should be noted that the $^3J_{H\varepsilon 1H\delta 1}$ coupling is 1.8 Hz for the tryptophan side chain, thus, for

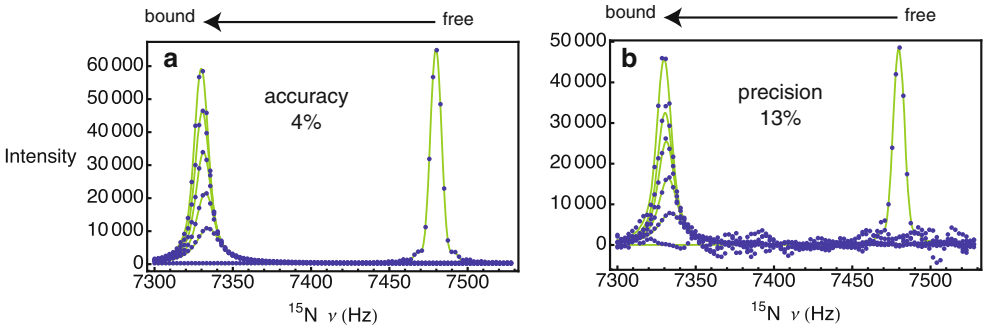

Fig. 10 GAMMA simulations for $K_D = 12$ μM and $k_{off} = 100$ s^{-1} using ^{15}N Method 2 (*blue circles*), with corresponding fits to the Bloch-McConnell equations (*green lines*) in absence (**a**) and the presence (**b**) of noise and concentration error. The accuracy or precision of the fitted k_{off} is given in the individual figure panels

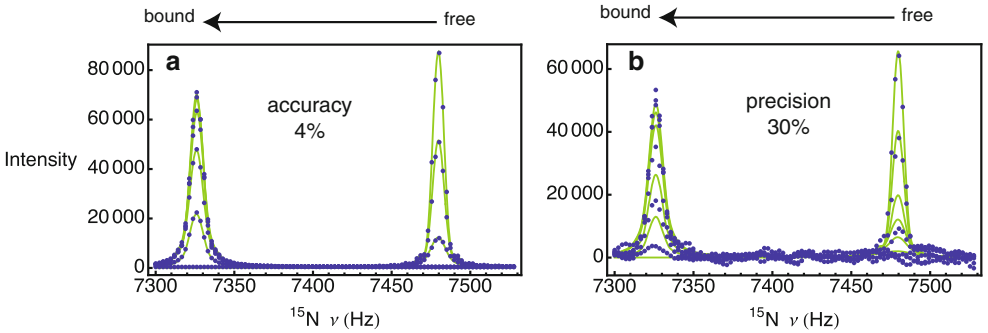

Fig. 11 GAMMA simulations for $K_D = 0.6$ μM and $k_{off} = 5$ s^{-1} for ^{15}N using a traditional titration, that is, Method 1 with P_T fixed at 0.5 mM (*blue circles*), with corresponding fits to the Bloch-McConnell equations (*green lines*) in absence (**a**) and the presence (**b**) of noise and concentration error. The accuracy or precision of the fitted k_{off} is given in the individual figure panels

line shape analyses of the experimental data for W33 $^1H_{\varepsilon 1}$ using the Bloch equations (Fig. 3c), this coupling can be ignored (Table 4). The accuracy for an actual value for k_{off} of 2,500 s^{-1} deteriorates to 16 % for the fitted value of 2,887 s^{-1}, in the presence of an unresolved coupling of 5 Hz (Fig. 12b). For a larger coupling of 10 Hz, employing the Bloch-McConnell equations gives rise to a 72 % error for the fitted value of 4,292 s^{-1} (Fig. 12d).

The above analysis indicates that if the Bloch equations are to be employed for analysis of $^1H^N$ spectral data in general, $^3J_{HH}$ couplings must be taken into account. There are potentially four different approaches to dealing with $^3J_{HH}$ couplings in the proton dimension of ^{1}H–^{15}N HSQC 2D NMR spectra. Homonuclear semi-selective shaped pulse decoupling during acquisition can be employed to decouple $^1H^N$ and $^1H_\alpha$, but suffers from substantial signal to noise losses due to intermittent receiver gating, and therefore, may be difficult to apply to protein systems undergoing chemical exchange (Hammarström and Otting 1994). Second generation pure shift homonuclear decoupling methods (Aguilar et al. 2010) offer another option, and have been extended to 2D HSQC NMR experiments (Sakhaii et al. 2009). However, the pure shift HSQC experiment provides less than half the signal to noise ratio of a regular HSQC. Uniform deuteration of the observed protein component (LeMaster 1994; Gardner and Kay 1998) is also a possible approach to minimize the impact of proton couplings on classical line shape analysis, as proton–deuteron coupling constants are reduced by a factor of $\gamma_H/\gamma_D \sim 6.5$ in comparison to proton–proton couplings, however, the $^1H^N$ resonance is split into a 1:1:1 triplet. Additionally, interference between dipolar and quadrupolar relaxation mechanisms for proton–deuteron pairs may give rise to asymmetric triplet patterns and line broadening, although these effects are expected to be small for proton–deuteron pairs that are separated by >2 Å (Grzesiek and Bax 1994). Finally, the doublet splitting arising from $^3J_{HH}$ coupling can be treated as the superposition of two uncoupled NMR resonances to a first approximation (Schmitt et al. 1995), but this approach requires measurement of the $^3J_{HH}$ coupling. However, accurate kinetics can be achieved without having to resort to protein perdeuteration, decoupling techniques, or density matrix formulations. For example, using GAMMA simulations for Method 1 (Table 1, $k_{off} = 2{,}500$ s^{-1}) with an unresolved $^3J_{HNH\alpha}$ of 5 Hz, the accuracy can be improved from 16 to

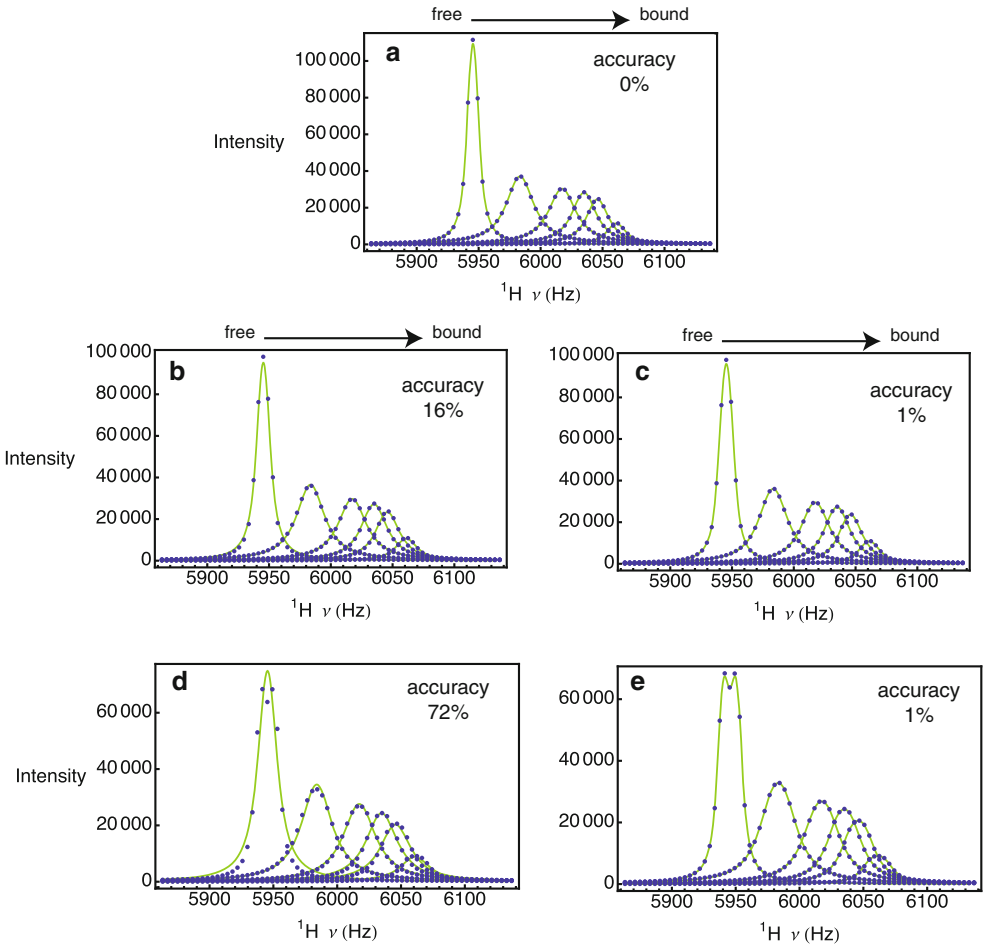

Fig. 12 GAMMA simulations for $K_D = 300$ μM and $k_{off} = 2{,}500$ s^{-1} using ^{1}H Method 1 (*blue circles*), with corresponding fits to the Bloch-McConnell equations (*green lines*) in presence of an unresolved 1.8 Hz coupling constant (**a**), in the presence of an unresolved 5.0 Hz coupling constant (**b**) in the presence of an unresolved 5.0 Hz coupling constant fit to the Bloch-McConnell equations modified to account for weak coupling according to Eq. 12 (**c**), in the presence of a partially resolved and unresolved 10 Hz coupling constant (**d**) and in the presence of a partially resolved and unresolved 10 Hz coupling constant fit to the Bloch-McConnell equations modified to account for weak coupling according to Eq. 12 (**e**). The accuracy of the fitted k_{off} is given in the individual figure panels

1 % (Figs. 12b and c). For a partially resolved and unresolved 10 Hz coupling, the accuracy is improved from 72 to 1 % (Figs. 12d and e).

Systematic errors in line shape analyses of NMR-monitored chemical shift titrations

Systematic error adversely impacts accuracy, and is insidious for highly precise line shape parameters, as the precision may be mistaken for high accuracy. However, as we have shown, a thorough Monte Carlo error analysis, including checks on parameter bias, may be helpful to identify potential systematic errors, which may arise from the values of R^0_{2A}, R^0_{2B}, and K_D that are used in line shape analyses. For example, a ±10 % error on the value of R^0_{2A} used in the line shape analysis of the GAMMA simulation for W33 ^{1}H$_{\varepsilon 1}$ using Method 1 (Table 3), directly translates into a systematic error of ±10 % on the value of the fitted k_{off}. Similarly, ±10 % error on the value of K_D gives a systematic error of ±11 % on the fitted value of k_{off}. Thus, knowledge of the errors on the values of K_D and R^0_{2A} establishes limits on the accuracy and precision of the k_{off}. For our implementation of line shape analysis, Monte Carlo simulations indicate that concentration error and noise in the FID give rise to a ±5 % error on the magnitude of R^0_{2A} when it is determined through fitting the free resonance peak to the Bloch-McConnell equations for $p_A = 1$. Thus, potential systematic errors for R^0_{2A} are about the same as the accuracy for k_{off}, and only half the precision of k_{off}, indicating that the fitted k_{off} will be accurate with respect to systematic errors in R^0_{2A}.

In general, for weak protein–ligand interactions in the fast exchange regime, dissociation constants determined from fits of chemical shift changes to 1:1 binding isotherms

are subsequently used in line shape analyses according to the relationship $k_{on} = k_{off}/K_D$, eliminating the need to fit one of the interaction rate constants. As previously discussed, we recently developed methods to determine precise K_D values from chemical shift titrations (Markin and Spyracopoulos 2012). For these experimental titrations, the standard deviations for the average per residue K_D value of Methods 1 and 2 are 6 and 11 %, respectively (Table 5, Markin and Spyracopoulos 2012). The precision in the K_D value for Method 2 is about the same as the precision in the k_{off} value. Thus, in a worst-case scenario, the fitted k_{off} value would have a systematic error close to the value of $\pm 1\sigma$ of the precision. However, the accuracy remains acceptable, as it would fall within one standard deviation of the experimental precision.

Theoretical accuracy and precision of K_D values from NMR-monitored chemical shift titrations

In addition to conducting line shape analyses, the ^{1}H and ^{15}N spectra (Figs. 5, 6, 7, 8, 9 and 10) from the GAMMA simulations we designed with different k_{off} values and protein and ligand concentrations given in Tables 1 and 2, were also used to assess the theoretical range for the accuracy and precision in K_D values determined from chemical shift titrations. We fit ^{1}H and ^{15}N line shapes calculated using GAMMA simulations for Methods 1 and 2, as well as a traditional titration, or Method 1 with P_T fixed at 0.5 mM, and various k_{off} values (Tables 7, 8) to the

Table 9 Theoretical accuracy and precision for K_D values from ^{15}N chemical shift titrations simulated with GAMMA

k_{off} (s^{-1})	Actual K_D (μM)	Fitted K_D M1[a] (μM)	Fitted K_D M2[b] (μM)	Fitted K_D M1-trad[c] (μM)
100	12	n.d.[d]	5 ± 1	n.d.
			56 (±8) %[e]	
500	60	200 ± 52	45 ± 5	34 ± 41
		233 (±87) %	25 (±8) %	43 (±68) %
1,000	120	135 ± 23	113 ± 9	142 ± 56
		13 (±19) %	6 (±8) %	18 (±47) %
15,000	1,800	1,840 ± 150	1,820 ± 90	1,840 ± 160
		2 (±8) %	1 (±5) %	2 (±9) %

[a] M1 indicates Method 1 with protein and ligand concentrations in Table 1

[b] M2 indicates Method 2 with protein and ligand concentrations in Table 2

[c] M1-trad indicates Method 1, with P_T fixed at 0.5 mM and ligand concentrations in Table 1

[d] Not determined

[e] Accuracy and precision are given as percentages of the absolute difference between the actual and fitted K_Ds, precision is given in parentheses

Table 10 Theoretical accuracy and precision for K_D values from ^{1}H chemical shift titrations simulated with GAMMA

k_{off} (s^{-1})	Actual K_D (μM)	Fitted K_D M1[a] (μM)	Fitted K_D M2[b] (μM)	Fitted K_D M1-trad[c] (μM)
1,500	180	195 ± 28	182 ± 14	217 ± 61
		8 (±16) %[d]	1 (±8) %	21 (±34) %
15,000	1,800	1,830 ± 170	1,830 ± 110	1,860 ± 180
		2 (±9) %	2 (±6) %	3 (±10) %

[a] M1 indicates Method 1 with protein and ligand concentrations in Table 1

[b] M2 indicates Method 2 with protein and ligand concentrations in Table 2

[c] M1-trad indicates Method 1, with P_T fixed at 0.5 mM and ligand concentrations in Table 1

[d] Accuracy and precision are given as percentages of the absolute difference between the actual and fitted K_Ds, precision is given in parentheses

Lorentzian line shape (Eq. 15) to determine chemical shifts, which were subsequently fit to 1:1 binding isotherms as previously described (Markin and Spyracopoulos 2012) to extract K_D values (Tables 9, 10). For $k_{on} = 8.33 \times 10^6$ M^{-1} s^{-1}, and k_{off} values of 100 and 500 s^{-1}, the magnitude of k_{ex} ($k_{on}[L] + k_{off}$) at the various protein:ligand concentration ratios, ranges from 1,033 s^{-1} to 8,861 s^{-1}. For a chemical shift difference between the free and bound states of 150 Hz, the angular frequency, $\Delta\omega$, is 942 rad s^{-1}. Thus, k_{ex} ranges from the intermediate ($k_{ex} \sim |\Delta\omega|$) to fast ($k_{ex} > |\Delta\omega|$) exchange regimes. As shown in Table 9, for ^{15}N, the accuracy in the K_D for all titration methods at k_{off} values of 100–500 s^{-1} is generally poor, no better than 25 %. Therefore, whilst the accuracy and precision of line shape analyses conducted at these k_{off} values is generally good (Table 7), large systematic errors in the fitted K_D values limit the accuracy of line shape analysis.

One solution to this problem is to employ isothermal titration calorimetry to determine K_D values as the intermediate exchange regime is approached for a given protein–ligand interaction (Ghai et al. 2012). Alternatively, the experimental design of chemical shift titrations using Method 2 avoids protein:ligand ratios wherein extensive line broadening is observed. Furthermore, for a given K_D, smaller $\Delta\omega$ values translate into narrower resonances during the titration, raising the possibility that the combination of a chemical shift titration conducted according to Method 2, with an analysis of K_D values determined from residues with different $\Delta\omega$ values can give a more accurate estimate of K_D. Therefore, we conducted simulations of T49 ^{15}N chemical shift titrations with the Bloch-McConnell equations for Methods 1 and 2, and a traditional titration, that is, Method 1 with $P_T = 0.5$ mM, using a k_{off} value of 500 s^{-1}. To test the lower limit of applicability, a titration with a slower k_{off} value of 100 s^{-1} using Method 2 was also

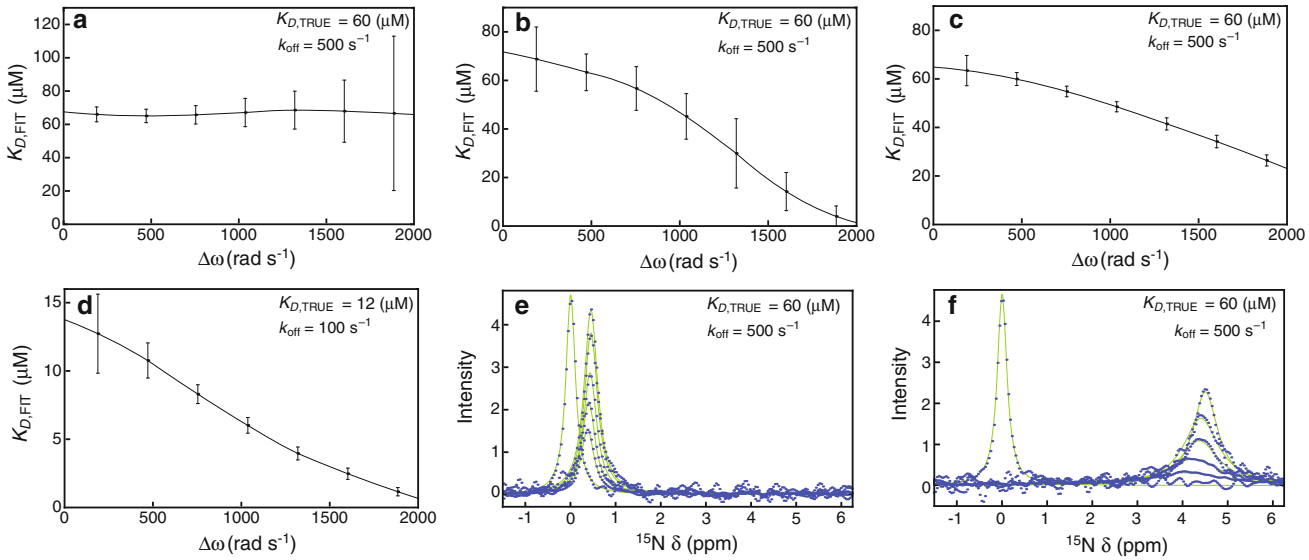

Fig. 13 Accuracy and precision of K_D values determined from Monte Carlo simulations of ^{15}N chemical shift titrations for (**a**) Method 1, (**b**) a traditional titration (Method 1 with $P_T = 0.5$ mM), and (**c**, **d**) Method 2. In **a**–**d**, the lines through the points are interpolated with a 2nd order polynomial. Representative spectra from simulated titrations (*blue circles*) and fits to the Lorentizan line shape (*green line*) are shown for Δω values of (**e**) 188.5 and (**f**) 1,885.0 rad s^{-1}

simulated as this method avoids much of the broadening that would be observed at protein:ligand ratios used in Method 1 or a traditional titration. The protein and ligand concentrations used with $k_{off} = 100$ and 500 s^{-1} are given in Tables 1 and 2. The bound chemical shift was varied to allow a range of Δω to be assessed (188.5, 471.2, 754.0, 1,036.7, 1,319.5, 1,602.2, 1,885.0 rad s^{-1}). Chemical shifts at the various protein:ligand ratios were obtained from the simulated titrations by fitting the spectral data to the Lorentzian line shape function. The mean value and the associated error for the optimized K_D at each Δω were obtained by generating an ensemble of 100 spectra per titration point through the addition of random noise to each point of FIDs calculated using the Bloch-McConnell equations. Each FID in the ensemble was Fourier transformed, and the resulting spectrum was fit to the Lorentzian line shape in order to obtain the chemical shift for the various titration points. These chemical shifts were subsequently fit to 1:1 binding isotherms (Eq. 6, Markin and Spyracopoulos 2012), to optimize the values of the adjustable parameters K_D and Δω. The results show that the accuracy of the fitted K_D improves with decreasing Δω for a variety of chemical shift titration methods (Fig. 13). Importantly, extrapolation of K_D as a function of the free and bound chemical shift difference to $\Delta\omega = 0$, allows for determination of a more accurate value for K_D if the titration data include some spectra within the intermediate exchange regime. This regime represents the lower limit of exchange for which chemical shift titrations can be used to fit K_D values, as a result of broadening and incomplete averaging of the free and bound peaks to a single resonance.

In general, Fig. 13 shows that for chemical shift titrations in which some titration points are in the intermediate exchange regime, the accuracy of the fitted K_D value deteriorates with increasing chemical shift difference between the free and bound states. This is mainly a result of increased line broadening due to increasing Δω (Fig. 13 b, c, d and a representative spectrum in Fig. 13f). As Δω decreases, the line broadening decreases, and the accuracy of K_D increases, as chemical shifts can be more accurately determined for narrower resonances (compare Fig. 13e, f). Importantly, as shown in Fig. 13e, for small Δω values, even in the presence of FID noise, the corresponding small chemical shift changes during a titration can be determined accurately using Method 2. Interpolating K_D values to $\Delta\omega = 0$ is feasible only when resonances from multiple protein residues are observed to shift to varying degrees in the spectra; however, this is often the case for protein:protein or protein:ligand interactions monitored by ^{1}H–^{15}N HSQC 2D NMR spectra, using uniformly ^{15}N-labelled protein as the observed component.

Within the lower range of the fast exchange regime, or $k_{ex} > |\Delta\omega|$, $k_{on} = 8.33 \times 10^6$ M^{-1} s^{-1} and k_{off} values of 1,000 and 1,500 s^{-1}, the accuracy and precision in the fitted K_D values is good for ^{1}H and ^{15}N using Methods 1 and 2 (19 % or better, Tables 9, 10). However, for the traditional method of conducting a titration (P_T fixed at 0.5 mM), the precision is poor, not better than 34 %. Thus, within the lower end of the fast exchange regime, the accuracy and precision of Methods 1 and 2 facilitate the determination of both the thermodynamics and kinetics of protein:ligand interactions.

The very fast exchange regime, or $k_{ex} \gg |\Delta\omega|$, with $k_{on} = 8.33 \times 10^6$ M^{-1} s^{-1} and $k_{off} = 15{,}000$ s^{-1}, corresponds to k_{ex} values ranging from $\sim$16,000 to 24,000 s^{-1}, depending on the protein:ligand ratio. In this exchange regime, GAMMA simulations indicate that the accuracy in the K_D value determined from the various chemical shift titrations for ^{1}H and ^{15}N is excellent, 3 % or better, and the precision is 10 % or better, for all titration methods (Tables 9, 10). These results establish that protein–ligand titrations monitored by ^{1}H–^{15}N HSQC 2D NMR spectroscopy represent a powerful approach for accurate and precise determination of the thermodynamics, that is K_D values, or populations, as well as kinetics of 1:1 protein–ligand interactions within the fast exchange regime.

Conclusions

We recently developed two chemical shift titration methods for the measurement of precise K_D values for 1:1 protein ligand interactions (Markin and Spyracopoulos 2012). In this study, we demonstrate that experimental line shape analyses conducted using these methods have an accuracy of <5 %, and a precision of 13 % in the fitted value of k_{off}. In addition, an analysis of potential systematic errors in the values of R^0_{2A} and K_D indicates that the accuracy of the experimental line shape analysis as implemented in this work may range from half the precision at best, to being about the same as the precision at worst, at a level of $\pm 1\sigma$. The theoretical range of kinetics for which line shape analysis is applicable was established using quantum mechanical simulations with the magnetic resonance toolkit GAMMA. These simulations demonstrate that line shape analysis provides reasonably accurate and precise k_{off} values over a wide range spanning 100–15,000 s^{-1}. Furthermore, theoretical simulations indicate that the applicability of line shape analysis to the lower range of k_{off} values, in the intermediate exchange regime, may be facilitated by more accurate K_D measurements, obtained by NMR-monitored chemical shift titrations where the dependence of K_D on the magnitude of chemical shift difference between the free and bound states is extrapolated to $\Delta\omega = 0$. The demonstrated level of accuracy and precision for k_{off} can be expected to be valuable for interpreting biological kinetics in the fast exchange regime for protein–protein interaction networks, where a modest change in the magnitude of a given on or off-rate due to a disease relevant mutation may lead to substantial changes in the populations of downstream protein complexes in a signaling cascade.

Acknowledgments This research was supported by the Canadian Institutes of Health Research (grant MOP 110964). L.S. is an Alberta Innovates—Health Solutions Senior Scholar, C.J.M. is the recipient of an Alberta Innovates—Health Solutions Studentship. We thank the Canadian National High Field NMR Centre (NANUC) for use of the facilities. Operation of NANUC is funded by the Natural Science and Engineering Research Council of Canada and the University of Alberta.

References

Aguilar JA, Faulkner S, Nilsson M, Morris GA (2010) Pure shift ^{1}H NMR: resolution of the resolution problem? Angew Chem Int Ed 49:3901–3903

Arai M, Ferreon JC, Wright PE (2012) Quantitative analysis of multisite protein-ligand interactions by NMR: binding of intrinsically disordered p53 transactivation subdomains with the TAZ2 domain of CBP. J Am Chem Soc 134:3792–3803

Bain AD (2003) Chemical exchange in NMR. Prog Nucl Mag Res Sp 43:63–103

Baldo JH, Halford SE, Patt SL, Sykes BD (1975) Stepwise binding of small molecules to proteins. Nuclear magnetic resonance and temperature jump studies of binding of 4-(*N*-Acetylaminoglucosyl)-*N*-Acetylglucosamine to lysozyme. Biochemistry 14: 1893–1899

Bax A, Grzesiek S (1993) Methodological advances in protein NMR. Acc Chem Res 26:131–138

Binsch G (1969) A unified theory of exchange effects on nuclear magnetic resonance line shapes. J Am Chem Soc 91:1304–1309

Bodenhausen G, Ruben DJ (1980) Natural abundance nitrogen-15 NMR by enhanced heteronuclear spectroscopy. Chem Phys Lett 69:185–189

Cavanagh J (2007) Protein NMR spectroscopy: principles and practice. Academic Press, Boston

Covert MW, Leung TH, Gaston JE, Baltimore D (2005) Achieving stability of lipopolysaccharide-induced NF-κB activation. Science 309:1854–1857

Fischer JJ, Jardetzky O (1965) Nuclear magnetic relaxation study of intermolecular complexes. The mechanism of penicillin binding to serum albumin. J Am Chem Soc 87:3237–3244

Gardner KH, Kay LE (1998) The use of ^{2}H, ^{13}C, ^{15}N multidimensional NMR to study the structure and dynamics of proteins. Annu Rev Biophys Biomol Struct 27:357–406

Gelis I, Bonvin AMJJ, Keramisanou D, Koukaki M, Gouridis G, Karamanou S, Economou A, Kalodimos CG (2007) Structural basis for signal-sequence recognition by the translocase motor SecA as determined by NMR. Cell 131:756–769

Ghai R, Falconer RJ, Collins BM (2012) Applications of isothermal titration calorimetry in pure and applied research: survey of the literature from 2010. J Mol Recognit 25:32–52

Greenwood AI, Rogals MJ, De S, Lu KP, Kovrigin EL, Nicholson LK (2011) Complete determination of the Pin1 catalytic domain thermodynamic cycle by NMR lineshape analysis. J Biomol NMR 51:21–34

Grzesiek S, Bax A (1994) Interference between dipolar and quadrupolar interactions in the slow tumbling limit: a source of line shift and relaxation in ^{2}H-labeled compounds. J Am Chem Soc 116:10196–10201

Günther UL, Schaffhausen B (2002) NMRKIN: simulating line shapes from two-dimensional spectra of proteins upon ligand binding. J Biomol NMR 22:201–209

Gutowsky HS, Saika A (1953) Dissociation, chemical exchange, and the proton magnetic resonance in some aqueous electrolytes. J Chem Phys 21:1688–1694

Haglund K, Di Fiore PP, Dikic I (2003) Distinct monoubiquitin signals in receptor endocytosis. Trends Biochem Sci 28:598–603

Hammarström A, Otting G (1994) Improved spectral resolution in ^{1}H NMR spectroscopy by homonuclear semiselective shaped pulse decoupling during acquisition. J Am Chem Soc 116:8847–8848

Hammes GG (2000) Thermodynamics and kinetics for the biological sciences. Wiley-Interscience, New York

Hoult DI (1978) The NMR receiver: a description and analysis of design. Prog Nucl Mag Res Sp 12:41–77

Johnson PE, Creagh AL, Brun E, Joe K, Tomme P, Haynes CA, McIntosh LP (1998) Calcium binding by the N-terminal cellulose-binding domain from *Cellulomonas fimi* β-1,4-glucanase CenC. Biochemistry 37:12772–12781

Kay LE, Keifer P, Saarinen T (1992) Pure absorption gradient enhanced heteronuclear single quantum correlation spectroscopy with improved sensitivity. J Am Chem Soc 114:10663–10665

Kern D, Kern G, Scherer G, Fischer G, Drakenberg T (1995) Kinetic analysis of cyclophilin-catalyzed prolyl cis/trans isomerization by dynamic NMR spectroscopy. Biochemistry 34:13594–13602

Korchuganov DS, Nolde SB, Reibarkh MY, Orekhov VY, Schulga AA, Ermolyuk YS, Kirpichnikov MP, Arseniev AS (2001) NMR study of monomer-dimer equilibrium of barstar in solution. J Am Chem Soc 123:2068–2069

Kovrigin EL (2012) NMR line shapes and multi-state binding equilibria. J Biomol NMR 53:257–270

LeMaster DM (1994) Isotope labeling in solution protein assignment and structural analysis. Prog Nucl Mag Res Sp 26:371–419

Lian L-Y, Roberts GCK (2011) Protein NMR spectroscopy: practical techniques and applications. Wiley, Chichester

Marintchev A, Frueh D, Wagner G (2007) NMR methods for studying protein–protein interactions involved in translation initiation. Methods Enzymol 430:283–331

Markin CJ, Spyracopoulos L (2012) Increased precision for analysis of protein-ligand dissociation constants determined from chemical shift titrations. J Biomol NMR 53:125–138

Markin CJ, Xiao W, Spyracopoulos L (2010a) Mechanism for recognition of polyubiquitin chains: balancing affinity through interplay between multivalent binding and dynamics. J Am Chem Soc 132:11247–11258

Markin CJ, Saltibus LF, Kean MJ, McKay RT, Xiao W, Spyracopoulos L (2010b) Catalytic proficiency of ubiquitin conjugation enzymes: balancing pK_a suppression, entropy, and electrostatics. J Am Chem Soc 132:17775–17786

McConnell HM (1958) Reaction rates by nuclear magnetic resonance. J Chem Phys 28:430–431

McKay RT, Tripet BP, Pearlstone JR, Smillie LB, Sykes BD (1999) Defining the region of troponin-I that binds to troponin-C. Biochemistry 38:5478–5489

McKenna S, Hu J, Moraes T, Xiao W, Ellison MJ, Spyracopoulos L (2003) Energetics and specificity of interactions within Ub•Uev•Ubc13 human ubiquitin conjugation complexes. Biochemstry 42:7922–7930

Morris GA, Freeman R (1979) Enhancement of nuclear magnetic resonance signals by polarization transfer. J Am Chem Soc 101:760–762

Palmer AG, Cavanagh J, Wright PE, Rance M (1991) Sensitivity improvement in proton-detected 2-dimensional heteronuclear correlation NMR spectroscopy. J Magn Reson 93:151–170

Palmer AG, Kroenke CD, Loria JP (2001) Nuclear magnetic resonance methods for quantifying microsecond-to-millisecond motions in biological macromolecules. Method Enzymol 339:204–238

Petrini JH (2007) Cell signaling. A touching response to damage. Science 316:1138–1139

Rao BDN (1989) Nuclear magnetic resonance line shape analysis and determination of exchange rates. Methods Enzymol 176:279–311

Rintala-Dempsey AC, Santamaria-Kisiel L, Liao Y, Lajoie G, Shaw GS (2006) Insights into S100 target specificity examined by a new interaction between S100A11 and annexin A2. Biochemistry 45:14695–14705

Rogers MT, Woodbrey JC (1962) Proton magnetic resonance study of hindered internal rotation in some substituted N, N-dimethylamides. J Phys Chem 66:540–546

Sakhaii P, Haase B, Bermel W (2009) Experimental access to HSQC spectra decoupled in all frequency dimensions. J Magn Reson 199:192–198

Schmitt TH, Zheng ZW, Jardetzky O (1995) Dynamics of tryptophan binding to *EscherichiacoliTrp* repressor wild type and AV77 mutant: an NMR study. Biochemistry 34:13183–13189

Shriver JW, Sykes BD (1981) Energetics and kinetics of interconversion of two myosin subfragment-1•adenosine 5′-diphosphate complexes as viewed by phosphorus-31 nuclear magnetic resonance. Biochemistry 20:6357–6362

Smith SA, Levante TO, Meier BH, Ernst RR (1994) Computer simulations in magnetic resonance. An object-oriented programming approach. J Magn Reson, Ser A 106:75–105

Sutherland IO (1972) The investigation of the kinetics of conformational changes by nuclear magnetic resonance spectroscopy. Annu Rep NMR Spectrosc 4:71–235

Tugarinov V, Kay LE (2003) Quantitative NMR studies of high molecular weight proteins: application to domain orientation and ligand binding in the 723 residue enzyme malate synthase G. J Mol Biol 327:1121–1133

Tugarinov V, Kay LE (2005) Methyl groups as probes of structure and dynamics in NMR studies of high-molecular-weight proteins. ChemBioChem 6:1567–1577

Vasavada KV, Kaplan JI, Rao BDN (1980). Density matrix theory of ABC $\rightleftarrows$ A'B' + C' chemical exchange: application to ^{31}P NMR spectra of interconverting enzyme bound reactants and products of phosphoryl transfer enzymes. J Magn Reson 41: 467–482